Cellular/Molecular

A Family of Nonclassical Class I MHC Genes Contributes to Ultrasensitive Chemodetection by Mouse Vomeronasal Sensory Neurons

Trese Leinders-Zufall,[1]* Tomohiro Ishii,[2,3]* Pablo Chamero,[1] Philipp Hendrix,[1] Livio Oboti,[1] Andreas Schmid,[1] Sarah Kircher,[1] Martina Pyrski,[1] Sachiko Akiyoshi,[2] Mona Khan,[2] Evelien Vaes,[2] Frank Zufall,[1] and Peter Mombaerts[2]

[1]Department of Physiology, University of Saarland School of Medicine, 66421 Homburg, Germany, [2]Max Planck Research Unit for Neurogenetics, 60438 Frankfurt, Germany, and [3]Department of Cell Biology and Center for Brain Integration Research, Tokyo Medical and Dental University, Graduate School of Medical and Dental Science, Bunkyo-ku, Tokyo 113-8510, Japan

The mouse vomeronasal organ (VNO) has a pivotal role in chemical communication. The vomeronasal sensory neuroepithelium consists of distinct populations of vomeronasal sensory neurons (VSNs). A subset of VSNs, with cell bodies in the basal part of the basal layer, coexpress *Vmn2r* G-protein-coupled receptor genes with *H2-Mv* genes, a family of nine nonclassical class I major histocompatibility complex genes. The *in vivo*, physiological roles of the *H2-Mv* gene family remain mysterious more than a decade after the discovery of combinatorial *H2-Mv* gene expression in VSNs. Here, we have taken a genetic approach and have deleted the 530 kb cluster of *H2-Mv* genes in the mouse germline by chromosome engineering. Homozygous mutant mice (ΔH2Mv mice) are viable and fertile. There are no major anatomical defects in their VNO and accessory olfactory bulb (AOB). Their VSNs can be stimulated with chemostimuli (peptides and proteins) to the same maximum responses as VSNs of wild-type mice, but require much higher concentrations. This physiological phenotype is displayed at the single-cell level and is cell autonomous: single V2rf2-expressing VSNs, which normally coexpress *H2-Mv* genes, display a decreased sensitivity to a peptide ligand in ΔH2Mv mice, whereas single V2r1b-expressing VSNs, which do not coexpress *H2-Mv* genes, show normal sensitivity to a peptide ligand in ΔH2Mv mice. Consistent with the greatly decreased VSN sensitivity, ΔH2Mv mice display pronounced deficits in aggressive and sexual behaviors. Thus, *H2-Mv* genes are not absolutely essential for the generation of physiological responses, but are required for ultrasensitive chemodetection by a subset of VSNs.

Key words: **accessory olfactory system; chemodetection; chromosome engineering; major histocompatibility complex; pheromone; vomeronasal receptor**

Introduction

The mouse vomeronasal epithelium (VNE) is characterized by a tripartite organization of vomeronasal sensory neurons (VSNs; Ishii and Mombaerts, 2008). VSNs with cell bodies in the apical layer of the VNE coexpress G-protein-coupled receptor genes of the *Vmn1r* repertoire (previously referred to as *V1R* or *V1r* genes) and the G-protein subunit *Gαi2*. VSNs with cell bodies in the basal VNE layer coexpress genes of the unrelated *Vmn2r* repertoire (*V2R* or *V2r* genes) and the G-protein subunit *Gαo*. The basal layer is subdivided into apical and basal parts based on expression of nine nonclassical class I major histocompatibility complex (MHC) genes (Adams and Luoma, 2013) termed *H2-Mv* genes (Ishii et al., 2003; Loconto et al., 2003). VSNs in the basal layer coexpress one of the 115 genes of the *Vmn2r* family ABD with one to six of the seven genes of the *Vmn2r* family C (Ishii and Mombaerts, 2011; Silvotti et al., 2011).

In the decade since the initial reports about *H2-Mv* genes and their VSN-specific, combinatorial expression patterns, little progress has been made in understanding the *in vivo*, physiological roles of H2-Mvs. No knock-out mice have been reported. Evidence for H2-Mvs promoting surface or functional Vmn2r expression is from heterologous cells and by overexpression (Loconto et al., 2003; Dey and Matsunami, 2011). Chemicals that stimulate basal VSNs are peptides or small proteins (Chamero et al., 2012): class I MHC-binding peptides and other urinary peptides (Leinders-Zufall et al., 2004, 2009; Sturm et al., 2013), exocrine gland-secreting peptide 1 (ESP1; Kimoto et al., 2005; Haga

Received Jan. 14, 2014; revised Feb. 26, 2014; accepted March 1, 2014.

Author contributions: T.L.-Z., T.I., F.Z., and P.M. designed research; T.L.-Z., T.I., P.C., P.H., L.O., A.S., S.K., M.P., S.A.-N., and M.K. performed research; T.L.-Z., T.I., E.V., F.Z., and P.M. analyzed data; T.L.-Z., T.I., F.Z., and P.M. wrote the paper.

This work was supported by the Deutsche Forschungsgemeinschaft (Grant SPP 1392 to T.L.-Z., F.Z., and P.M.; Grant SFB 894 to T.L.-Z. and F.Z.; and Grant CH920/2-1 to P.C.; PY90/1-1 to M.P.), the National Institutes of Health (T.L.-Z., T.I., F.Z., and P.M.), the Volkswagen Foundation (T.L.-Z.), and the European Research Council (Advanced Grant ORGENECHOICE to P.M.). T.L.-Z. is a Lichtenberg Professor of the Volkswagen Foundation. We thank Wei Tang and Duancheng Wen for injecting ES cells into blastocysts; Thomas Boehm for peptides; Roberto Tirindelli and Kazushige Touhara for antibodies; Petra Hammes, Michael Konzmann, and Katja Langenfeld for technical assistance; and Bernd Bufe for discussions.

The authors declare no competing financial interests.

*T.L.-Z. and T.I. contributed equally to this work.

Correspondence should be addressed to either of the following: Peter Mombaerts, Max Planck Research Unit for Neurogenetics, Max-von-Laue-Strasse 3, 60438 Frankfurt, Germany, E-mail: peter.mombaerts@biophys.mpg.de; or Frank Zufall, University of Saarland School of Medicine, Department of Physiology, Kirrberger Strasse, Building 58, 66421 Homburg, Germany, E-mail: frank.zufall@uks.eu.

DOI:10.1523/JNEUROSCI.0186-14.2014

 0270-6474/14/345121-13$15.00/0

et al., 2007, 2010), and major urinary proteins (MUPs; Chamero et al., 2007, 2011). These chemostimuli are all related to the identity of the organism that emits the molecules. The high sensitivity (picomolar thresholds) and exquisite specificity (single amino acid changes) of some *Vmn2r*-expressing VSNs for class I MHC peptides (Leinders-Zufall et al., 2004, 2009) suggest that VSNs detect these peptides via H2-Mvs. However, VSNs expressing the *Vmn2r* gene *V2r1b* do not coexpress *H2-Mv* genes but can be activated by class I MHC peptides (Leinders-Zufall et al., 2009).

The *H2-Mv* genes form a single gene cluster within a 530 kb region of the *MHC* locus on chromosome 17 that contains no other genes. Here, we have used the strategy of chromosome engineering (Ramírez-Solis et al., 1995) to delete this region in mouse embryonic stem (ES) cells and generate mouse strains. We performed Ca^{2+} imaging of genetically labeled VSNs in acute VNO slices, local field potential recordings of the VNE, and Ca^{2+} imaging of dissociated VSNs. These approaches reveal a consistent phenotype: the maximum amplitude of the responses to chemoligands remains the same, but the threshold and EC_{50} values are increased by 8- to 34-fold. ΔH2Mv males and females exhibit severe deficits in aggressive and sexual behaviors. The deficit in male–male aggression can be overcome by increasing the concentration of urinary ligand.

Thus, *H2-Mv* genes are not absolutely essential for the generation of physiological responses to chemostimuli by certain basal VSNs, but are required for ultrasensitive chemodetection by these cells.

Materials and Methods

Chromosome engineering. DNA sequences were obtained from BAC clones of mouse 129/SvEv genomic origin. As homology arms of the *M10.2* targeting vector: nt 36283661–36285669 (mouse genome assembly GRCm38) and nt 36277188–36283666; as probe for Southern blot for the *M10.2* targeting vector: nt 36285671–36286169; as homology arms of the *M10.6* targeting vector: nt 36810861–36815770 and nt 36815765–36819293; as probe for Southern blot for the *M10.6* targeting vector: nt 36810361–36810860; as probe for Cre-mediated recombination: human *Hprt* gene amplified with primers, 5′-*GAACCTGCCAGTCTGATAGG* and 5′-*GCGACCTTGACCATCTTTGG*, from the *Hprt (5′)-loxP-neo* cassette (Ramírez-Solis et al., 1995). Chromosome engineering was performed as described previously (Ramírez-Solis et al., 1995; Del Punta et al., 2002a). The deletion is 532,098 bp, from position 36283667 to 36815764 (GRCm38). Replacement vectors for each end of the *H2-Mv* gene cluster, *M10.2* and *M10.6* loci, were constructed using the cassettes *Hprt (5′)-loxP-neo* and *puro-loxP-Hprt (3′)*, respectively. The vectors were electroporated consecutively into AB2.2 cells, which are derived from an *Hprt*-deficient 129/SvEv blastocyst. Clones with the two targeted events were electroporated with the Cre-expression plasmid pOG231. Cells that underwent recombination between the *loxP* sites and thus express reconstituted functional *Hprt* were selected in hypoxantine-aminopterin-thymidine medium. ES cells were injected into C57BL/6 blastocysts and male chimeras were crossed to 129/SvEv females (Taconic).

Deletion of all nine *H2-Mv* genes was confirmed by PCR using the following primers: outside the cluster at *M10.2* locus, 5′-*GGAGTCACAGCTTTCCTGTG* and 5′-*GAAATACATCTAATGTAAAGACGTG*; outside the cluster at *M10.6* locus, 5′-*TGCAGACTCAGTGTCTGTGAG* and 5′-*TATTCATGTATACAAATCAGTGAATTG*; *M1*, 5′-*AATCCAGAAGACTTATGGCTG* and 5′-*CCAAAGGCCAGGAATCGATG*; *M9*, 5′-*ATCCAGGAAACATATGGCTG* and 5′-*CCAAAGTTCAGGTATTGAAG*; *M11*, 5′-*ATCCAGAGAAGGTATGGCTG* and 5′-*CCATATTCCAGCTCTGTGAG*; *M10.1*, 5′-*TATCACACCCTGCAGGAAGT* and 5′-*GTAAGTCTTCCTCCGTTTTG*; *M10.2*, 5′-*TATCACACCCTGCAGGAAGT* and 5′-*GTAGGTCCTCCAGCCTTCCG*; *M10.3/M10.5*, 5′-*TATCACACCCTGCAGGAAGT* and 5′-*GTAAGTCTTCCACCTTTCTG*; *M10.4*, 5′-*TATCACACCCTGCAGGAAGT* and 5′-*GTAAGTCCTCCAACCTTCTG*; *M10.6*, 5′-*TATCACACCCTGCAGGAAGT* and 5′-*GTAAGTCCTCCAACTTTCTG*.

ΔH2Mv mice are available from The Jackson Laboratory: strain A in an inbred 129/Sv background as stock JR#6730 and strain name 129-Del(17)4Mom/1MomJ; strain A after at least seven backcrosses to C57BL/6J as JR#8097 and B6.129-Del(17)4Mom/1MomJ; strain C in 129/Sv as JR#6731 and 129-Del(17)5Mom/1MomJ; and strain C backcrossed to C57BL/6J as JR#8098 and B6.129-Del(17)5Mom/1MomJ. Results were obtained with strain C.

Mouse experiments were performed in accordance with NIH guidelines and the German Animal Welfare Act, European Communities Council Directive 2010/63/EU, and the institutional ethical and animal welfare guidelines of the Max Planck Institute of Biophysics, the Max Planck Research Unit for Neurogenetics, and the University of Saarland. Approval came from the Institutional Animal Care and Use Committee of The Rockefeller University, the Veterinäramt of the City of Frankfurt, and the Animal Welfare Committee of the University of Saarland.

In situ *hybridization and immunohistochemistry*.

Male mice aged 10 weeks were used unless mentioned otherwise. Dissection and sectioning, and *in situ* hybridization (ISH) were performed as described previously (Ishii et al., 2004). RNA probes were as described previously (Ishii et al., 2003; Ishii and Mombaerts, 2008). Immunohistochemistry (IHC) was performed as described previously (Ishii and Mombaerts, 2008), except for IHC with anti-Go-VN4 and anti-V2R2 antibodies, which was done according to Martini et al. (2001). Primary antibodies were rabbit anti-Gαo antibody (Sc-387; Santa Cruz Biotechnology), mouse anti-Gαi2 antibody (MAB3077; Millipore), rabbit anti-Synapsin I antibody (ab1543; Millipore), chicken anti-GFP (AB13970; Abcam), rabbit anti-Go-VN4 and anti-V2R2 antibodies (gifts from Roberto Tirindelli, University of Parma, Italy), and anti-V2Rp5 antibodies (gift from Kazushige Touhara, University of Tokyo, Japan). Secondary antibodies were Alexa Fluor 488 goat anti-rabbit IgG (A11008; Invitrogen), Alexa Fluor 555 donkey anti-rabbit IgG (A31572; Invitrogen), RRX donkey anti-mouse IgG (715-296-150; Jackson ImmunoResearch), cyanine 5 donkey anti-rabbit IgG (711-175-152; Jackson ImmunoResearch), and FITC donkey anti-chicken IgG (703-095-155; Jackson ImmunoResearch). Sections were analyzed with a Zeiss LSM 510 confocal microscope.

Cell counts and measurements. For counts of V2rf2-GFP cells, coronal 20 μm cryosections were cut throughout the VNO. The number of cells labeled with intrinsic GFP fluorescence was counted every sixth section. For counts from ISH experiments, 14 μm cryosections were cut throughout the VNO from 129/Sv mice. The number of labeled cells was counted every 18th section. For measurements of the areas of the Gαi2- and Gαo-positive layers, coronal 14 μm cryosections were cut throughout the VNO from 129/Sv mice. The stained areas were measured every 18th section using Zeiss ZEN 2011 software and the ratio was determined. For cell counts and measurements, images were assigned a random number and images for WT and ΔH2Mv mice were mixed. Images were analyzed without knowledge of the genotype.

NanoString. NanoString gene expression analysis was as described previously (Khan et al., 2011, 2013; Vaes et al., 2014). Normalization of the data was performed with regard to five reference genes, which are the most stable among samples and are expressed in VSNs: *Ano2*, *Cnga4*, *Gnai2*, *Omp*, and *Trpc2*. The NanoString probe sequences and data have been deposited in NCBI's Gene Expression Omnibus (Edgar et al., 2002) and are accessible through GEO accession number GSE54061.

Gene nomenclature. V2rf1, *V2rf2*, *V2rf3*, *V2r1b*, and *V1rb1* are the earlier *Vmn2r* gene names and were incorporated into the names of the gene-targeted strains before the official nomenclature was changed to *Vmn2rxxx*. These genes correspond to, respectively, *Vmn2r82*, *Vmn2r81*, *Vmn2r80*, *Vmn2r26*, and *Vmn1r50*. The former name for *Vmn2r* genes is *V2R* (or *V2r*) genes. For *H2-Mv* genes, we use the official nomenclature (Mouse Genome Informatics and Ensembl), which corresponds to the nomenclature of Ishii et al. (2003). The V2R2 antigen (Martini et al., 2001) is now known to correspond collectively to the protein products of the family-C *Vmn2r* genes.

Chemostimuli. Immediately before use, ligands were diluted in HEPES-buffered extracellular solution consisting of the following (in

mM): 145 NaCl, 5 KCl, 10 HEPES, 1 $MgCl_2$, 1 $CaCl_2$, adjusted to pH 7.2 (NaOH) and 300 mOsm (glucose). Unless stated otherwise, chemicals were obtained from Sigma-Aldrich. Most MHC peptides were designed according to known binding specificities of MHC molecules and were chemically synthesized, purified, and verified by mass spectroscopy (MALDI-TOF, provided by Thomas Boehm). Peptides were initially dissolved in PBS at a concentration of 1–10 mM and stored frozen. Peptide preparations did not contain free amino acids. f-MFFINTLTL, MFFINTLTL, f-MFFINILTL, f-MLF, and SIINFEKL (Genscript) were initially dissolved in bicarbonate-containing bath solution to give 100 μM stock solutions. Isoamylamine and 2-heptanone were prepared with <0.1% DMSO. Of the five MUPs expressed in male C57BL/6 mice, we used MUP3, MUP8, MUP17, and MUP25 (nomenclature of Logan et al., 2008), which are also known as MUP3, MUP8, MUP15, and MUP18 (Mudge et al., 2008). Recombinant ESP1 and MUPs, collection of fresh urine, and urine fractionation were as described previously (Chamero et al., 2011). To obtain the high molecular weight (HMW) fraction, male urine was size fractionated by centrifugation using Microcon 10 kDa molecular weight cutoff ultrafiltration columns (Millipore). The column retentate was washed three times with one volume of PBS and resuspended in the same initial urine volume (HMW) or in 1/4 of the initial volume (4 × HMW).

Physiology. Calcium imaging in VNO tissue slices was as described previously (Leinders-Zufall et al., 2000, 2004, 2009; Sturm et al., 2013). Mice were 2–8 months old and of either sex. Intracellular Ca^{2+} in VSNs of ΔV2rf2-lacZ mice was monitored using fluo-4/AM (Invitrogen) and LacZ was visualized as described previously (Leinders-Zufall et al., 2007). The final concentration in the experimental chamber was 4.6 μM fluo-4/AM, 0.01% Pluronic F-127, and 0.1% DMSO. Local field potentials were recorded from the luminal VNO surface as described previously (Leinders-Zufall et al., 2000, 2004; Zufall et al., 2002; Chamero et al., 2011; Leinders-Zufall and Zufall, 2013). Stimulation with control buffer was performed at the beginning of each experiment and between exposures to chemostimuli. Ratiometric Ca^{2+} imaging of dissociated VSNs using Fura-2/AM and statistical analyses were as described previously (Chamero et al., 2011).

VNO whole-mount imaging. For imaging of VNE microvilli and the M10.2::GFP fusion protein (Ishii and Mombaerts, 2008), we used the VNO whole-mount preparation for EVG recordings (Leinders-Zufall et al., 2000; Zufall et al., 2002), with the difference that the opened skull was embedded in 4% agarose to prevent movement. We adapted previously established imaging methods (Leinders-Zufall et al., 2007; Rivière et al., 2009). Microvilli of WT mice were visualized using the plasma membrane dye CellMask Orange at 1: 500 for 3 min (Invitrogen). Images were taken with a Leica TCS SP5 confocal microscope and a 20×1.0 water-immersion objective (HCX APO L). 3D reconstructions were produced from confocal image *z*-stacks using the plugin Z Project of ImageJ.

AOB c-Fos activation. Adult females (129/Sv or ΔH2Mv, 2–4 months old) were singly housed in fresh cages for at least 3 h and then stimulated with 20 μl of vehicle (20 mM Tris-HCl, pH 8.0) with or without recombinant ESP1 (1 or 100 μM) onto the oronasal groove (3 mice per stimulus condition and strain). After stimulus take-up, mice were kept for additional 90 min in their cages before transcardial perfusion and c-Fos immunohistochemistry were performed. AOB c-Fos expression was detected using the avidin-biotin amplification method (Vectastain ABC-Elite; Vector Laboratories). Free-floating cryosections (30 μm, sagittal plane) were sequentially incubated in 3% H_2O_2 in PBS for 10 min, in blocking solution (PBS pH 7.4, 4% normal horse serum, 0.3% Triton X-100) for 1 h, in primary rabbit c-Fos antibody (1:20,000, Ab-5 PC38; Calbiochem) diluted in blocking solution for 2 d at 4°C, in biotinylated goat anti-rabbit IgG (1:200; Vector Laboratories) for 1 h, and in avidin/biotin HRP-complex (Vector Laboratories) for 90 min. If not otherwise noted, incubations were performed at room temperature. Immunoreactivity was visualized with 0.05 g/L DAB (Sigma-Aldrich) and 0.015% H_2O_2 in PBS. Bright-field images were acquired on a BX61 microscope attached to a DP71 camera (Olympus) and minimally adjusted in contrast and brightness using Adobe Photoshop Elements 10. c-Fos-positive neurons were quantified along the mediolateral axis of the AOB. Neurons in the mitral cell layer of both rostral and caudal portions were counted.

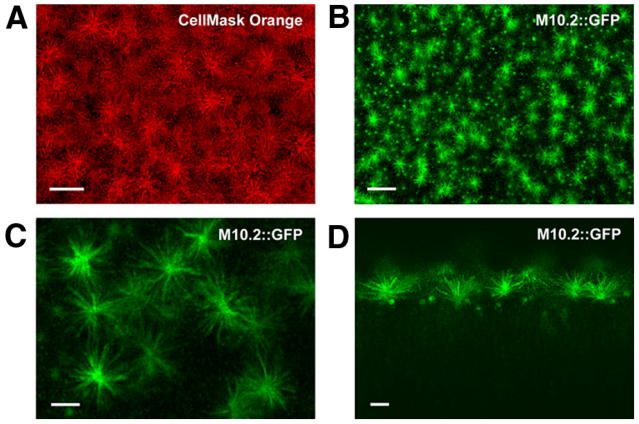

Figure 1. M10.2::GFP enrichment in VSN microvilli. ***A***, Confocal imaging of microvilli covering the VNE surface. Microvilli were visualized in red using the plasma membrane dye CellMask Orange in an *ex vivo* whole-mount VNO preparation of a WT mouse (en face). Scale bar, 10 μm. ***B***, Confocal imaging of M10.2::GFP fluorescence in whole mount. En face view of the surface of VNE reveals a homogeneous distribution of M10.2::GFP VSNs. Individual microvilli emanating from a given dendritic knob are clearly visible. A *z*-stack of 60 images was taken ($\Delta z = 0.7904$ μm) and a maximum *z*-projection was produced. Scale bar, 20 μm. ***C***, Single confocal image, en face view, showing M10.2::GFP^+ microvilli at higher resolution. Scale bar, 5 μm. ***D***, Single confocal image, side view. The M10.2::GFP fusion protein is strongly enriched in the microvilli. Scale bar, 5 μm.

Behavioral testing. Resident-intruder and maternal aggressive behavior tests were as described previously (Chamero et al., 2007, 2011). The pup retrieval assay was as described previously (Chamero et al., 2011), with the difference that four instead of five pups were used. To measure female receptive behavior, adult sexually naive female 129/Sv or ΔH2Mv mice (8–12 weeks old) were singly housed for 1 week. Their estrous cycle was assessed to use only females in the estrous or proestrous phase. Adult males (sexually experienced, C57BL/6) were introduced into the home cage of the female. During the 30 min test session, female responses to male mounts or intromissions were scored as either totally unreceptive with kicking, rearing, or fleeing or receptive lordosis posture with some degree of dorsiflexion of the vertebral column. Males were not used on consecutive days. The same males were used with both female genotypes. Video analyses were done randomly and blindly for all behavioral assays. Results were statistically analyzed as in Chamero et al. (2011).

Statistics. Data were analyzed using statistical software NCSS 2004. The unpaired Student's *t* test was used for measuring the significance of difference between two independent distributions. Multiple groups were compared using the ANOVA with the Fisher's least significant difference (LSD) as a *post hoc* comparison. A Benjamini and Hochberg algorithm was applied to adjust for multiple statistical comparisons of NanoString data (Khan et al., 2011, 2013; Vaes et al., 2014). Unless otherwise stated, results are presented as means ± SEM.

Results

M10.2::GFP is highly enriched in VSN microvilli

We examined the subcellular localization of M10.2 protein in mice with a gene-targeted mutation that results in the expression of a C-terminal M10.2::GFP fusion protein in cells that normally express the *M10.2* gene. This *H2-Mv* gene is expressed in 95% of VSNs that express *H2-Mvs* (Ishii and Mombaerts, 2008). We visualized all VSN microvilli in an ex vivo whole-mount VNO preparation using the plasma membrane dye CellMask Orange (Fig. 1*A*). An en face view of the VNE surface reveals a homogeneous and punctate distribution of M10.2::GFP-expressing VSNs (Fig. 1*B*,*C*). A side view illustrates the strong enrichment of M10.2::GFP protein in VSN microvilli (Fig. 1*D*). Another H2-Mv

protein, M10.5, is also confined to the tip of VSN dendrites (Loconto et al., 2003). We have therefore focused our studies on the chemosensory, dendritic functions of H2-Mvs.

Targeted deletion of the *H2-Mv* gene cluster

The cluster of nine *H2-Mv* genes occupies 530 kb at the telomeric end of the *MHC* locus on mouse chromosome 17 (Fig. 2*A*). There are no other annotated genes within this 530 kb region. This genomic organization provides the opportunity to design a clean deletion that encompasses all nine *H2-Mv* genes, but no other genes. We performed chromosome engineering in ES cells of line AB2.2, which is of 129/SvEv origin (Ramírez-Solis et al., 1995; Fig. 2*A*). ES cells carrying the 532,098 bp deletion were injected into blastocysts and germline transmission was obtained. ΔH2Mv mice are viable and fertile. PCR on genomic DNA of ΔH2Mv mice confirmed the absence of the nine *H2-Mv* genes from their genomic DNA, whereas sequences just outside of the engineered deletion (centromerically and telomerically) are retained (Fig. 2*B*).

Anatomical analysis of the VNO

We performed ISH and IHC on coronal sections of the VNOs of WT and ΔH2Mv mice in an inbred 129/Sv background (Fig. 2*C–K*). ISH with a mixture of *H2-Mv* probes reveals expression in the basal part of the basal VNE layer in WT mice and, as expected, not in ΔH2Mv mice (Fig. 2*C*). ISH with a pan-*MHC* probe does not give a signal in the basal VNE layer of ΔH2Mv mice (Fig. 2*D*), indicating that no other class I *MHC* genes are upregulated as compensation. IHC with anti-Go-VN4 antibodies (Martini et al., 2001; Fig. 2*E*), anti-V2R2 antibodies (Martini et al., 2001; Fig. 2*F*), or anti-V2Rp5 antibodies (Haga et al., 2010; Fig. 2*G*,*G*′) does not reveal overt differences in the intensity and subcellular location of the signals. The numbers of V2Rp5-immunoreactive cells are similar in WT and ΔH2Mv mice (data not shown). The region of the VSNs close to the dendritic tip shows similar immunoreactive signals in WT and ΔH2Mv mice; insets in Figure 2*E* are for anti-Go-VN4, a polyclonal antibody raised against a rat Vmn2r that cross-reacts with mouse Vmn2rs of clade III, which includes Vmn2r111 through Vmn2r117 (Silvotti et al., 2007).

We have not been able to reproduce the finding of severely compromised localization of anti-Go-VN4 immunoreactivity in the dendritic tips of VSNs from β2-microglobulin (β2M) knock-out mice (Loconto et al., 2003). Using the same antibody and the same strain of β2M knock-out mice, IHC patterns are indistinguishable and we detect no obvious difference in staining in β2M knock-out mice crossed with M10.2-IRES-tauVenus mice (data not shown).

ISH with *Gαi2* and *Gαo* probes reveals a normal pattern of interdigitating apical and basal layers of the VNE in ΔH2Mv mice (Fig. 2*H*). The ratio of the *Gαo/Gαi2* areas is 0.99 in WT and 0.93 in ΔH2Mv mice (Fig. 2*I*), which may reflect a minor decrease in basal VSN numbers at 10 weeks. We performed three-color ISH with probes for *Vmnr* genes that are expressed in the apical layer (probe *V1rb1*, labeling seven *Vmn1r* genes: *40*, *41*, *44*, *46*, *49*, *50*, *53*), in the apical part of the basal layer (probe *V2r1b*, labeling nine *Vmn2r* genes: *19* through *27*), and in the basal part of the basal layer (probe *V2rf1-3*, labeling three *Vmn2r* genes: *80*, *81*, *82*). In WT mice, >98% of cells labeled with the *V2rf1-3* probe coexpress *H2-Mv* genes at this age of 10 weeks compared with 0% for the *V1rb1* probe and <10% for the *V2r1b* probe (Ishii and Mombaerts, 2008). We find that the tripartite layering of the VNE is maintained in ΔH2Mv (Fig. 2*J*). Cell counts reveal no differences for the *V1rb1* and *V2r1b* probes and the number of cells reacting with the *V2rf1-3* probe shows a 25% decrease in ΔH2Mv mice at 10 weeks (Fig. 2*K*).

We analyzed intrinsic GFP fluorescence of VSNs in V2rf2-IRES-tauGFP mice (V2rf2-GFP; Ishii and Mombaerts, 2011), which are available only in a mixed 129/Sv × C57BL/6 genetic background. Cell bodies of V2rf2-GFP VSNs reside in the basal part of the basal VNE layer (Fig. 2*L*) and the intensity of the fluorescent signal per cell is identical in both backgrounds (data not shown). The number of V2rf2-GFP VSNs is decreased on average by 55% in the ΔH2Mv background, but cell counts in this mixed genetic background vary considerably among individual mice, with overlap among the two genotypes (Fig. 2*M*).

Thus, these anatomical analyses show that the VNE of ΔH2Mv mice is not altered in a drastic way, that the tripartite layering is maintained, and that there is a minor decrease in the number of basal VSNs at 10 weeks.

Anatomical analysis of the AOB

In the AOB, axons of VSNs terminate and coalesce into glomeruli. A cross of ΔH2Mv mice with OMP-tau-lacZ mice (Mombaerts et al., 1996), in which all mature VSNs can be stained blue with Xgal, reveals no overt differences in the shape or size of the AOB in whole mounts (Fig. 3*A*,*B*). A cross of ΔH2Mv mice with NP2-Δ mice (Walz et al., 2002), in which all apical VSNs express tauGFP, reveals a normal demarcation of the anterior (aAOB), which receives axons of GFP^+ VSNs from the posterior AOB (pAOB; Fig. 3*C*). IHC on sagittal AOB sections with antibodies against Gαi2 (aAOB) and Gαo (pAOB) confirms this normal demarcation in ΔH2Mv mice in an inbred 129/Sv background (Fig. 3*D*). V2rf2-GFP mice show GFP^+ glomeruli in the middle part of the pAOB in whole mounts (Fig. 3*E*) and there is no obvious difference in the number and location of GFP^+ glomeruli in the ΔH2Mv background (Fig. 3*F*). The fluorescence signal at GFP^+ glomeruli is lower and the size of these glomeruli is decreased in the ΔH2Mv background, which is consistent with a decreased number of V2rf2-GFP VSNs (Fig. 2*M*). IHC on AOB sections with antibodies against synapsin-1, a marker for presynaptic terminals, reveals normal staining in and around V2rf2 glomeruli in the ΔH2Mv background (Fig. 3*G*,*H*).

Thus, these analyses reveal no drastic anatomical differences in the AOB of ΔH2Mv mice and exclude a major role of ΔH2Mvs in the guidance of VSN axons to the AOB and in their coalescence into glomeruli.

NanoString analysis of gene expression

The NanoString platform enables multiplex analysis of gene expression in total RNA samples. We have previously designed specific NanoString probes for half of the odorant receptor gene repertoire (Khan et al., 2011). We have now designed specific NanoString probes for one-third of the *Vmn2r* gene repertoire based on the reference C57BL/6 genome sequence. CodeSet Chanel includes probes for 46 *Vmn2r* genes and the nine *H2-Mv* genes; due to the high homology of *Vmn2r* genes, we could not design specific probes for the other *Vmn2r* genes. We analyzed total RNA samples from VNO mucosae of 6 WT and 6 ΔH2Mv mice in a 129/Sv background aged 3 weeks and from 6 WT and 6 ΔH2Mv mice in a C57BL/6 background aged 8 weeks.

RNA counts for the nine *H2-Mv* genes are at background levels in ΔH2Mv mice at both ages (Fig. 4*A*,*C*), providing another assessment that these genes have been deleted from the genome. Of the 46 *Vmn2r* genes in CodeSet Chanel, 37 gave sufficient counts in WT mice at 3 weeks to be informative and 36

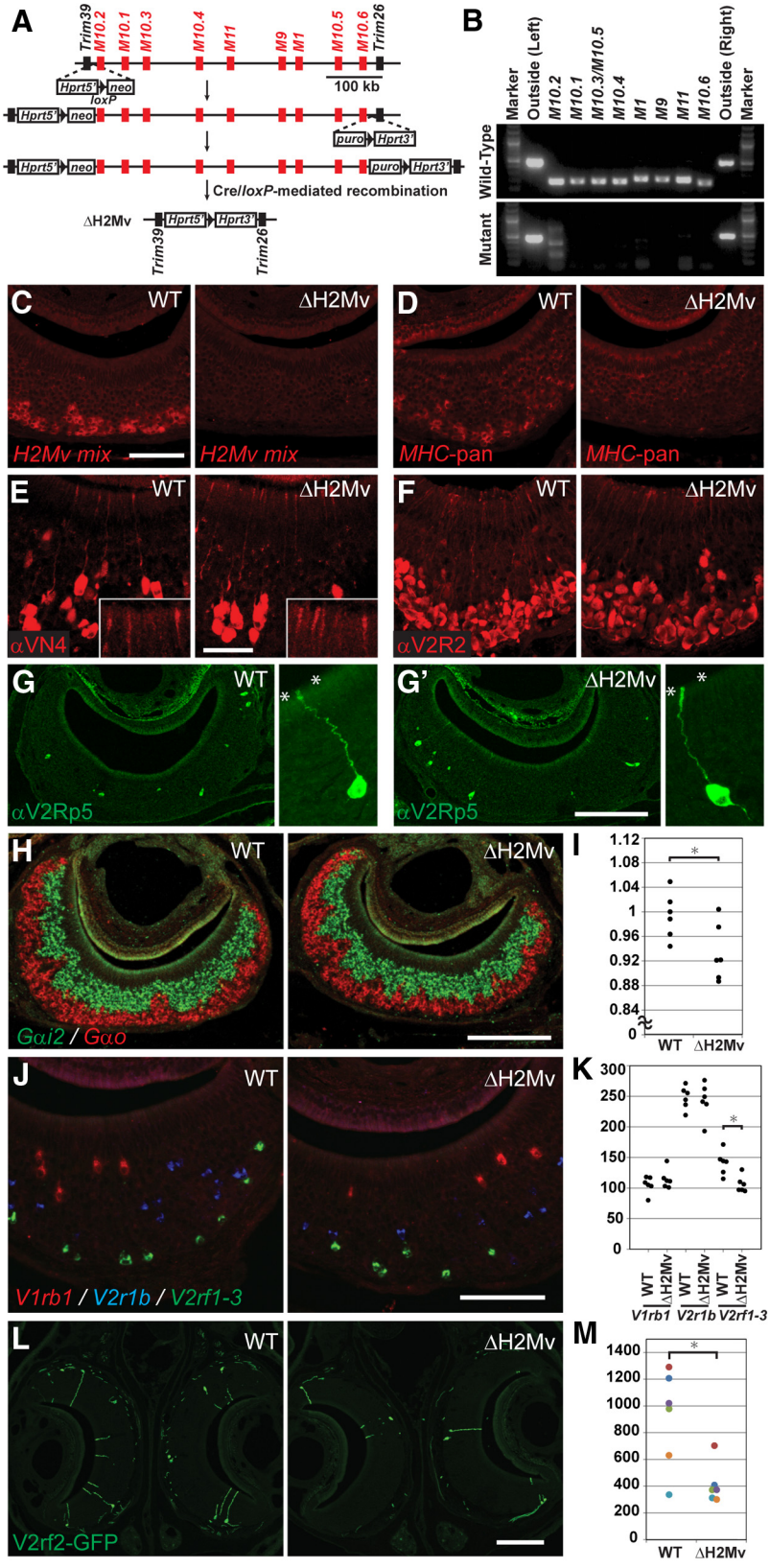

Figure 2. Targeted deletion of the *H2-Mv* cluster and histology of the VNO. ***A***, Chromosome engineering of the cluster of the nine *H2-Mv* genes on chromosome 17. Replacement vectors containing the *Hprt* exons 1–2 (5′)-*loxP-neo* sequence and the *puro-loxP-Hprt* exons 3–9 (3′) sequence were targeted to the *M10.2* (left) and *M10.6* (right) loci in ES cells of line AB2.2 by consecutive rounds of gene targeting. In the third and final round, transient expression of the Cre recombinase resulted in a deletion of the cluster by site-specific recombination between *loxP* sites. This deletion reconstitutes a functional *Hprt* gene, allowing for positive selection. ***B***, PCR analysis of genomic DNA with primers for each *H2-Mv* gene and for sequences outside of the cluster. ***C***, ISH with the mixed *H2-Mv* probe on coronal sections of the VNO of a WT and a ΔH2Mv mouse. Scale bar, 100 μm. ***D***, ISH with the *MHC-pan* probe from *H2-Q1* on coronal sections of the VNO of a WT and a ΔH2Mv mouse. ***E–F***, IHC with the anti-VN4 antibody (***E***) and the anti-V2R2 antibody (***F***) on coronal sections of the VNO of a WT and a ΔH2Mv mouse. The inset shows a higher-magnification view of the VNO surface. Scale bar, 50 μm. ***G***, ***G′***, IHC with the anti-V2Rp5 antibody on coronal sections of the VNO of a WT (***G***) and a ΔH2Mv mouse (***G′***). Right, Higher-magnification view of a labeled VSN. Asterisks indicate the apical surface of the VNE. Scale bar, 200 μm. ***H***, Two-color ISH with the *Gαi2* probe (green) and the *Gαo* probe (red) on coronal sections of the VNO of a WT and a ΔH2Mv mouse. Scale bar, 200 μm. ***I***, Ratio of *Gαo*-positive to *Gαi2*-positive areas. A dot represents the ratio for a single mouse. Six mice were analyzed for each genotype. There is a significant difference ($*p < 0.05$, $t_{(10)} = 2.45$, *t* test) between the ratio of 0.99 ± 0.04 (average ± SD) in WT mice compared with 0.93 ± 0.05 in ΔH2Mv mice. ***J***, Three-color ISH with the *V1rb1* probe (red), the *V2r1b* probe (blue), and the *V2rf1-3* probe (green) on coronal sections of the VNO of a WT mouse and a ΔH2Mv mouse. Note that only *V2rf1-3* genes are coexpressed with *H2-Mv* genes. Scale bar, 100 μm. ***K***, Numbers of ISH-positive neurons for each probe. Every 18th section throughout the VNE was analyzed. Raw counts for both VNOs are shown. Six mice were analyzed for each genotype-probe pair. *V1rb1* in WT, 105 ± 14 (average ± SD); *V1rb1* in ΔH2Mv, 115 ± 16; *V2r1b* in WT, 247 ± 18; *V2r1b* in ΔH2Mv, 243 ± 28. *V2rf1-3* in WT; 141 ± 19; *V2rf1-3* in ΔH2Mv; 106 ± 13. There is a significant difference between WT and ΔH2Mv for *V2rf1-3* ($*p < 0.05$, $t_{(10)} = 2.86$, *t* test). ***L***, Coronal sections of the VNO of a homozygous V2rf2-GFP mouse (WT) and a homozygous V2rf2-GFP, ΔH2Mv mouse (ΔH2Mv). Signals are from intrinsic fluorescence of GFP and signal intensity is identical in WT and ΔH2Mv backgrounds. Scale bar, 200 μm. ***M***, Number of V2rf2-GFP$^+$ VSNs per mouse. One mouse of each genotype (ΔH2Mv WT and mutant) per litter was analyzed of six litters total. A dot represents the total number of GFP$^+$ cells per mouse; colors of the dots represent different litters. There is a significant difference ($*p < 0.05$, $t_{(10)} = 3.12$, *t* test) between WT, 910 ± 362 (average ± SD), compared with ΔH2Mv, 411 ± 148. All samples and counts in ***C–M*** were from male mice aged 10 weeks, except for samples in ***G*** and ***G′***, which were from male mice aged 11 weeks.

in WT mice at 8 weeks. In 3-week old mice, there is no significant difference in expression of these 37 *Vmn2r* genes between ΔH2Mv and WT mice (Fig. 4*B*) based on a fold change of 1.3 (increased or decreased) and $p < 0.01$ (Khan et al., 2011, 2013; Vaes et al., 2014). In 8-week old mice, 30 of 36 *Vmn2r* genes show no significant difference between ΔH2Mv and WT mice (Fig. 4*D*). Of interest for further studies are *Vmn2r10* (counts in ΔH2Mv are 10% of WT), *Vmn2r14* (10%), and *Vmn2r70* (12%).

Thus, the assayable *Vmn2r* genes show no difference in RNA expression in ΔH2Mv mice compared with WT mice at 3 weeks and expression of the large majority of assayable *Vmn2r* genes is not affected at 8 weeks.

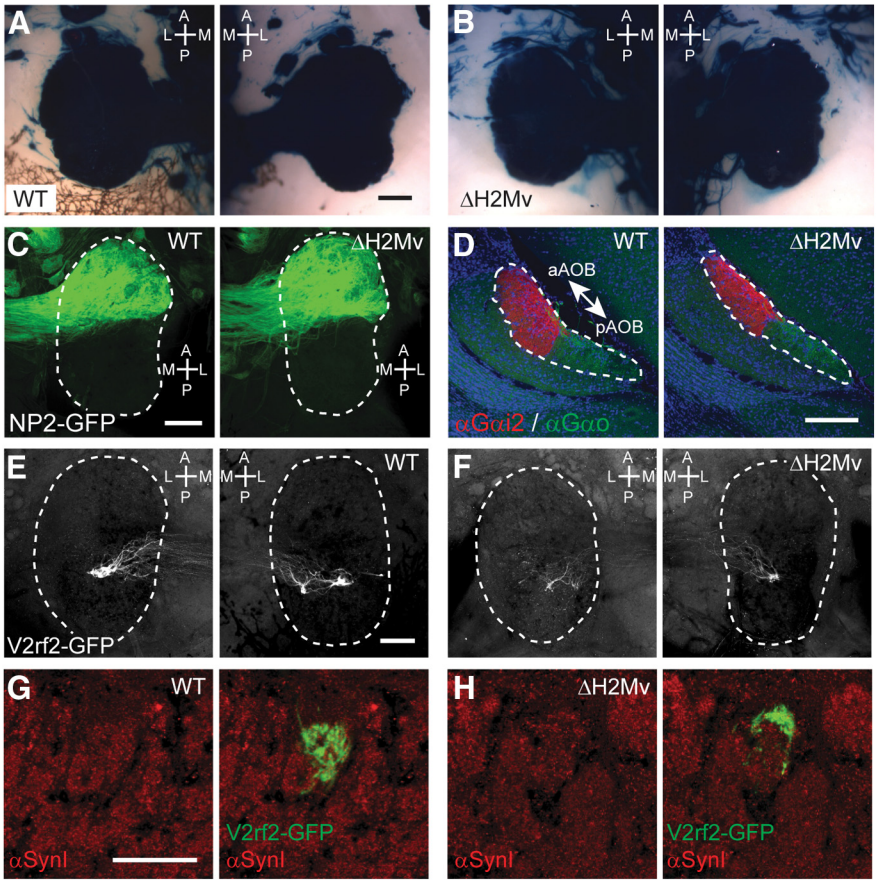

Figure 3. Axonal projections to the AOB. ***A***, ***B***, Whole-mount dorsal view of the AOB of a heterozygous OMP-tau-lacZ mouse (WT; ***A***) and a heterozygous OMP-tau-lacZ, ΔH2Mv mouse (***B***) stained with X-gal. A, Anterior; P, posterior; L, lateral; M, medial. Scale bar, 200 μm. ***C***, Dorsal view of whole mounts of a left AOB of a heterozygous NP2-GFP mouse (WT) and a heterozygous NP2-GFP, ΔH2Mv mouse. The area of the AOB is outlined with a stipple line. Scale bar, 200 μm. ***D***, IHC with an anti-Gαi2 antibody (red) and an anti-Gαo antibody (green) on sagittal sections of the AOB of a WT and a ΔH2Mv mouse. Sections were counterstained with TOTO-3 to visualize nuclei. The area of the AOB is outlined with a stipple line. aAOB, Anterior AOB; pAOB, posterior AOB. Scale bar, 200 μm. ***E***, ***F***, Dorsal view of whole mounts of left and right AOBs of an homozygous V2rf2- GFP mouse (WT; ***E***) and a homozygous V2rf2-GFP, ΔH2Mv mouse (ΔH2Mv; ***F***). The area of the AOB is outlined with a stipple line. Scale bar, 200 μm. ***G***, ***H***, IHC with an anti-Synapsin I antibody (red) on AOB sagittal sections from a homozygous V2rf2-GFP mouse (WT; ***G***) and a homozygous V2rf2-GFP, ΔH2Mv mouse (ΔH2Mv; ***H***). Scale bar, 50 μm. All samples were from male mice aged 10 weeks.

Rightward shift in concentration-response curves of single VSNs

We examined Ca^{2+} responses in labeled VSNs of V2rf2-IRES-tauGFP mice (Ishii and Mombaerts, 2011). These cells express *V2rf2* but no other family-ABD *Vmn2r* gene (Ishii and Mombaerts, 2011); *H2-Mv* genes (Ishii and Mombaerts, 2008); and the family-C gene *Vmn2r1* (Ishii and Mombaerts, 2011), which has normal NanoString counts at both 3 and 8 weeks (Fig. 4*B*,*D*). We loaded acute coronal VNO tissue slices with the Ca^{2+} indicator dye fura-red/AM (Leinders-Zufall et al., 2000, 2004, 2009). Figure 5*A* shows an example of red fluorescence in a GFP^+ cell, resulting in a yellow merge. Because no ligands had been identified for the V2rf2 receptor or for V2rf2-expressing VSNs, we tested a range of chemostimuli. We identified two distinct ligands for V2rf2-GFP VSNs: the MHC peptide SEIDLILGY and the formylated peptide f-MFFINTLTL (Fig. 5*B–D*). This formylated peptide is a natural ligand of mitochondrial or bacterial origin and activates VSNs in a *Gαo*-dependent manner (Chamero et al., 2011) and also some FPRs in heterologous cells (Bufe et al., 2012). Examples of Ca^{2+} responses in a single V2rf2-GFP cell (c4 in Fig. 5*D*) are shown in Figure 5*B* and summaries in Figure 5, *C* and *D*. Of 24 V2rf2-GFP cells exposed to the SEIDLILGY peptide, 12 (50%) responded, and, of 30 cells exposed to the f-MFFINTLTL peptide, 17 (57%) responded. Of 10 cells (c1-c10 in Fig. 5*D*) exposed to these peptides, 5 responded to both peptides and the other 5 cells responded to neither. The formyl group is not required for activity: MFFINTLTL stimulated 6/6 V2rf2-GFP cells (Fig. 5*D*,*E*). V2rf2-GFP cells did not respond to three other MHC peptides: SFVDTRTLL, KLYEQGSNK, and SIINFEKL (Fig. 5*B*,*D*). Neither did V2rf2-GFP cells respond to three recombinant major urinary proteins: rMUP3, rMUP8, or rMUP17 (Fig. 5*D*).

Next, we imaged labeled VSNs of ΔV2rf2-lacZ mice, in which the coding sequence of V2rf2 is partially deleted and replaced by taulacZ (Ishii and Mombaerts, 2011). Of 25 ΔV2rf2-lacZ cells, none responded to SEIDLILGY or f-MFFINTLTL; the normal KCl responses indicate that these cells were viable (Fig. 5*C*,*D*). We have reported similar findings about the necessity of an intact *Vmn2r* locus using ΔV2r1b-GFP cells and MHC peptides such as SYFPEITHI (Leinders-Zufall et al., 2009). Thus, V2rf2 is absolutely essential for the generation of Ca^{2+} responses to peptide ligands in cells that have chosen to express the *V2rf2* locus.

We then analyzed Ca^{2+} responses to peptides in V2rf2-expressing cells in the ΔH2Mv background. We find that 6/11 (55%) and 5/8 (63%) of V2rf2-GFP cells responded to, respectively, SEIDLILGY or f-MFFINTLTL (Fig. 5*C*). Therefore, H2-Mvs are not absolutely essential for physiological responses to be generated in V2rf2-expressing cells, in sharp contrast to V2rf2 itself. To determine whether H2-Mvs are required for ultrasensitive chemodetection of V2rf2-GFP cells, we produced concentration-response curves for SEIDLILGY and f-MFFINTLTL in single V2rf2-GFP cells in WT and ΔH2Mv backgrounds. We find that higher concentrations of SEIDLILGY are needed in the ΔH2Mv background to begin to detect Ca^{2+} responses (Fig. 5*F*). Importantly, the same maximum responses can be obtained, but with much higher concentrations of peptide ligand. There is thus a pronounced rightward shift of the concentration-response curves in the ΔH2Mv background: a 34-fold shift for SEIDLILGY (Fig. 5*G*) and a 25-fold shift for f-MFFINTLTL (Fig. 5*H*). The Hill coefficients do not seem to be altered in ΔH2Mv mice. As a further control, we compared concentration-response curves in single V2r1b-GFP cells (Del Punta et al., 2002b) stimulated with SYFPEITHI (Leinders-Zufall et al., 2009) in WT and ΔH2Mv backgrounds (Fig. 5*I*). Because *V2r1b* is not coexpressed with *H2-Mv* genes (Ishii and Mombaerts, 2008), there is no reason to expect a difference. Indeed, there is no sensitivity shift in V2r1b-GFP cells in the ΔH2Mv background, demonstrating that the ΔH2Mv phenotype is cell autonomous: the mutation affects sensitivity only of the VSNs that normally express *H2-Mv* genes. This experiment also argues against systemic or nonspecific effects of the mutation.

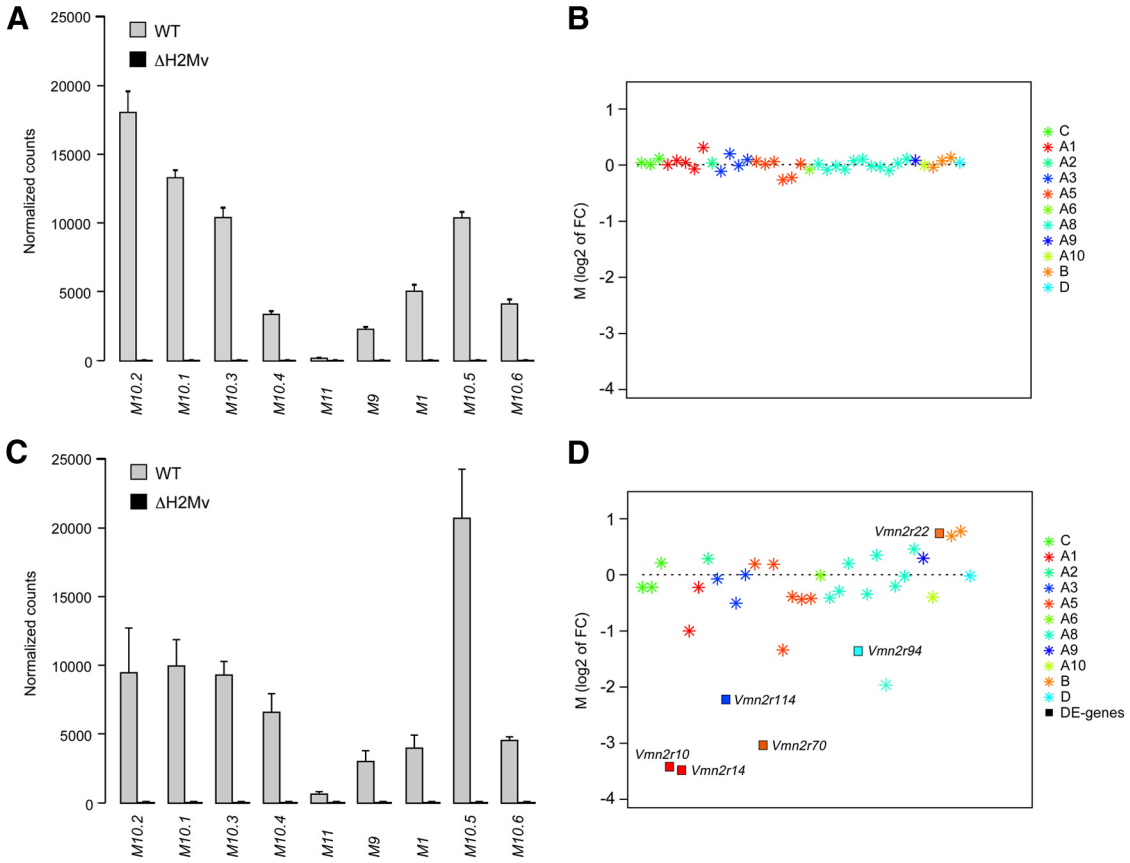

Figure 4. NanoString gene expression analysis. ***A***, Counts for each of the nine *H2-Mv* genes in ΔH2Mv and WT mice in a 129/Sv background at 3 weeks. Genes are arranged according to their position on chromosome 17. Note that the absolute values of counts in WT mice cannot be compared among *H2-Mv* genes due to differences in the efficiency of probe recovery and detection. ***B***, M-values plotted for the 37 informative *Vmn2r* genes in CodeSet Chanel at 3 weeks. M is the log2 of the fold change of counts in ΔH2Mv mice over the counts in WT mice. *Vmn2r* genes are arranged per family and then numerically within a family. Families are depicted in different colors. The black stipple line corresponds to an M value of 0, which represents no change in ΔH2Mv mice compared with WT mice. There are no differentially expressed *Vmn2r* genes. ***C***, Counts for each of the nine *H2-Mv* genes in ΔH2Mv and WT mice in a C57BL/6 background at 8 weeks. ***D***, M-values for the 36 informative *Vmn2r* genes at 8 weeks. Differentially expressed (DE) genes are indicated by filled squares and their names are annotated.

Thus, VSN sensitivity to peptide ligands is decreased in ΔH2Mv mice and thresholds and EC_{50} values are increased. It takes a much higher ligand concentration to cause a response in these cells, but eventually they do respond and ultimately they respond to the same maximum levels.

Electrovomerograms

To determine whether ligand-evoked receptor potentials are also decreased in ΔH2Mv mice, we recorded local field potentials from the surface of the VNE in an ex vivo whole-mount preparation: the electrovomerogram (EVG; Leinders-Zufall et al., 2000; Zufall et al., 2002). This electrophysiological method measures voltage changes that are the summation of the responses of a cell population in the vicinity of the recording pipette. We performed these experiments in inbred 129/Sv mice that are either WT or ΔH2Mv and tested additional ligands.

Figure 6*A* shows a summary of EVG peak amplitudes for eight ligands, each at a fixed concentration. Peak amplitudes for 5/6 ligands known to stimulate basal, *Vmn2r*-expressing VSNs and/or to depend on *Gαo* (Chamero et al., 2011) are strongly decreased in ΔH2Mv mice (ANOVA: $F_{(1,178)} = 23.22$, $p < 0.0001$). Only SYFPEITHI elicits similar peak amplitudes (LSD: $p = 0.13$), at the high, saturated concentration of 10^{-11} M. By contrast, ligands that are known to stimulate apical, *Vmn1r*-expressing VSNs (2-heptanone and isoamylamine) elicit equal peak amplitudes in WT and ΔH2Mv mice (LSD: $p = 0.61$ and 0.78, respectively), which is consistent with the absence of H2-Mv expression in these cells in WT mice; the phenotype of the ΔH2Mv mutation is cell autonomous.

Figure 6*B* shows an example of responses to rMUP25: the shape and peak amplitude of the responses are unaltered, but higher concentrations of rMUP25 are needed in the ΔH2Mv background to start to detect a response. Figure 6, *C–F*, shows concentration-response curves for four ligands: as was the case for single V2rf2-GFP cells, the maximum responses are the same and the Hill coefficients appear to be unaltered. The rightward shift ranges from 8- to 16-fold (Fig. 6*G*).

Thus, our EVG analyses confirm and extend the observations made in single V2rf2-GFP cells: sensitivity of the VNE is greatly decreased, threshold and EC_{50} values are increased, but the maximum responses are the same.

Ca^{2+} responses in dissociated VSNs

Next, we used ratiometric Ca^{2+} imaging with Fura-2/AM in populations of freshly dissociated VSNs (Chamero et al., 2007, 2011). We tested a series of dilutions of a mixture of natural ligands: the high molecular weight (HMW; >10 kDa) fraction of urine from C57BL/6 males. This preparation contains the five MUPs that C57BL/6 males express in their urine (Chamero et al., 2007; Logan et al., 2008; Mudge et al., 2008). These experiments afford a quantitation of the percentages of responding cells among the entire population of VSNs and a comparison of response maps

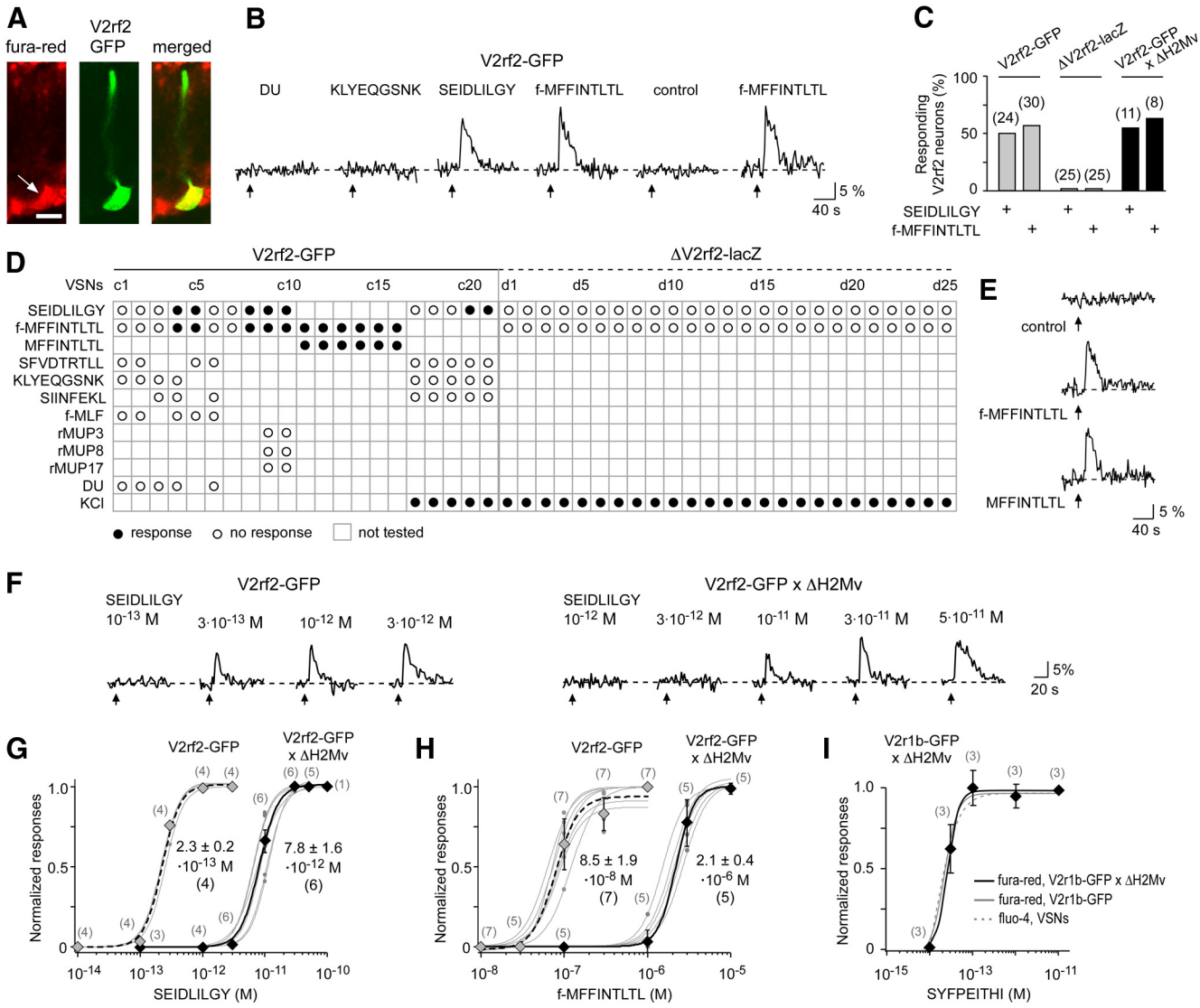

Figure 5. Calcium imaging in single V2rf2-GFP VSNs. ***A***, Confocal imaging of V2rf2-GFP VSNs in a coronal VNO slice loaded with the Ca^{2+} indicator dye Fura-red/AM (red, arrow). Merged image (yellow) shows that a V2rf2-GFP VSN (green) took up the Ca^{2+} dye. Scale bar, 10 μm. ***B***, Ca^{2+} responses of a single V2rf2-GFP cell (c4 in ***D***) to various stimuli. This cell detected the two peptides SEIDLILGY (10^{-9} M) and f-MFFINTLTL (10^{-7} M). Repeated presentations of the same stimuli indicate that Ca^{2+} peak responses were highly reproducible. DU, Diluted urine (1:100); KLYEQGSNK (10^{-9} M). A response is defined as a stimulus-dependent deviation in Ca^{2+} fluorescence that exceeds twice the SD of the mean of the baseline fluorescence noise. Arrows indicate the time points at which a 10 s stimulus application was turned on. Controls with stimulus buffer did not induce any response. ***C***, Bar histogram indicating response probabilities of three types of genetically labeled VSNs. V2rf2-GFP (24 mice): SEIDLILGY 10^{-12}, 10^{-11} and 10^{-9} M, f-MFFINTLTL 10^{-7} M; ΔV2rf2-lacZ (11 mice): SEIDLILGY 10^{-11} M, f-MFFINTLTL 10^{-6} and 3×10^{-6} M; V2rf2-GFP × ΔH2Mv (11 mice): SEIDLILGY 10^{-11} and 10^{-9} M, f-MFFINTLTL $3{\cdot}10^{-6}$ M. All concentrations used were in the saturating or near-saturating range of the concentration-response curves for that genotype. The number of cells tested is shown in brackets above each bar. ***D***, Response profiles of V2rf2-GFP and ΔV2rf2-lacZ VSNs. Concentrations used were as follows: SIINFEKL, 10^{-11} M; SEIDLILGY, SFVDTRTLL, KLYEQGSNK, 10^{-9} M; f-MFFINTLTL, MFFINTLTL, rMUP3, rMUP8, rMUP17, f-MLF, 10^{-7} M; DU, diluted urine, 1:100; KCl, 60 mM. Stimuli were delivered in random order. ***E***, Ca^{2+} responses to formylated (10^{-7} M) and nonformylated MFFINTLTL (10^{-7} M) in the same V2rf2-GFP VSN (c11). ***F***, Concentration dependency of SEIDLILGY-evoked Ca^{2+} responses imaged in individual V2rf2-GFP or V2rf2-GFP × ΔH2Mv VSNs. Stimuli were applied in consecutive order. ***G***, ***H***, Concentration-response curves constructed from Ca^{2+} peak responses. Each curve (gray) was obtained from a single V2rf2-GFP ($n = 11$) or V2rf2-GFP × ΔH2Mv VSN ($n = 11$) stimulated with SEIDLILGY (***G***) or f-MFFINTLTL (***H***). Relative changes in peak fluorescence ($\Delta F/F$) induced by a given stimulus (gray dots) were normalized to the maximum peak response measured in a given VSN to construct the curves. Curves are fits of the Hill equation combined with an iterative Levenberg–Marquardt nonlinear, least-squares fitting routine, defining threshold, EC_{50}, and saturation. Individual stimuli were tested in a 4 min trial with a 2 min gap between trials (illumination off). Cells were tested in 6–10 trials in total using controls and 5–6 distinct stimuli. Stimuli were tested 1–3 times/neuron. Mean values and their error bars (SD) of the responses to a given concentration are indicated by diamond symbol (gray: V2rf2-GFP; solid black: V2rf2-GFP × ΔH2Mv). The number of independent recordings is plotted in brackets near each symbol. The dashed and solid black curves represent the mean concentration-response curves of V2rf2-GFP and V2rf2-GFP × ΔH2Mv VSNs, respectively, fitted using all measured data points. EC_{50} value, SD, and number of cells (in brackets) are indicated. There is no significant difference in maximum responses to a given stimulus between V2rf2-GFP and V2rf2-GFP × ΔH2Mv (ANOVA: $F_{(3,21)} = 16.1$, $p = 0.62$): mean ± SEM (n): SEIDLILGY, 12.3 ± 1.2% (4) and 9.8 ± 0.5% (6); f-MFFINTLTL, 13.5 ± 4.2% (7), and 12.3 ± 1.3% (5). ***I***, Concentration-response curves constructed from Ca^{2+} peak responses of V2r1b-GFP × ΔH2Mv VSNs ($n = 3$) responding to SYFPEITHI. Mean values and their error bars (SD) of the responses to a given concentration are indicated by diamond symbols. For comparison are published data with randomly chosen VSNs of wild-type mice (Leinders-Zufall et al., 2004) and V2r1b-GFP VSNs (Leinders-Zufall et al., 2009); dotted and gray curves, respectively.

between WT and ΔH2Mv mice. We examined inbred 129/Sv mice, which are WT or ΔH2Mv.

Figure 7 reports on imaging Ca^{2+} responses in 2061 cells from 10 WT mice and 1905 cells from 10 ΔH2Mv mice. Figure 7, *A* and *B*, shows examples of Fura-2 ratio images with three dilutions of the HMW fraction. Responsive cells are depicted in magenta. Examples of Ca^{2+} responses in individual cells with various dilutions of the HMW fraction are shown in Figure 7, *C* and *D*. The

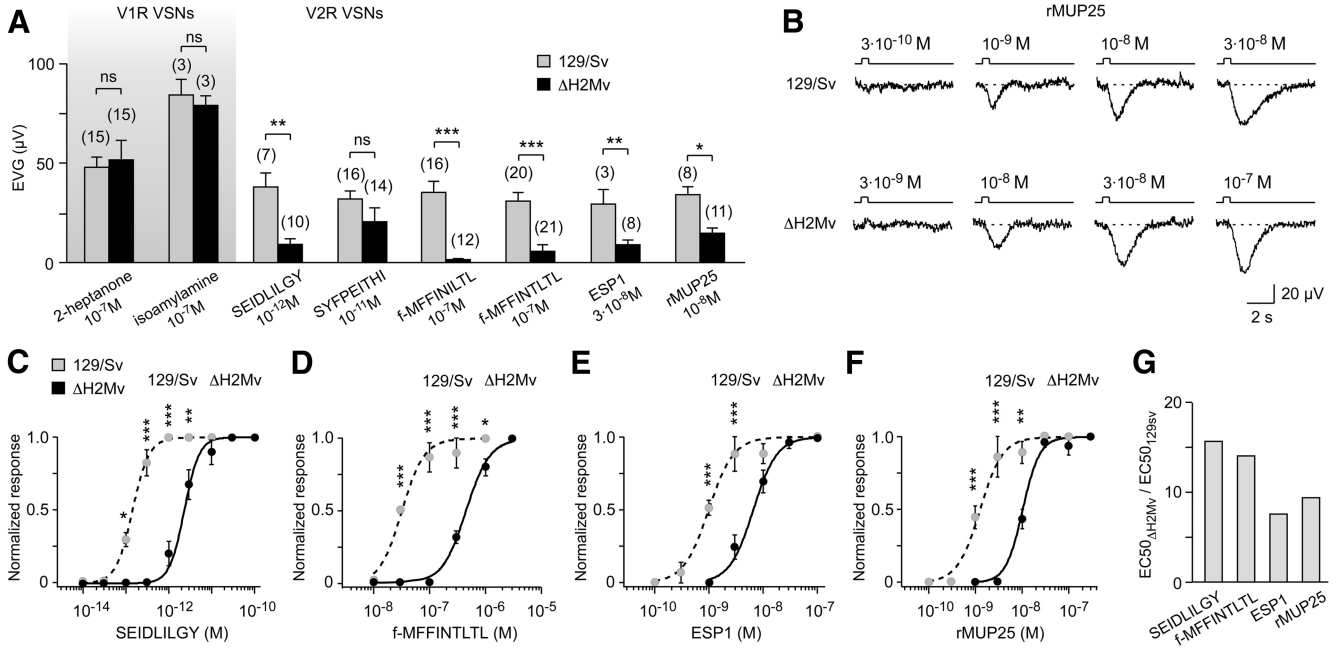

Figure 6. Electrovomerograms. ***A***, Histogram summarizing EVG peak responses to eight ligands recorded from 129/Sv and ΔH2Mv mice. EVG responses to various ligands known to stimulate VSNs in the basal, *Vmn2r*-expressing layer are decreased in ΔH2Mv mice (ANOVA: $F_{(1,178)} = 23.22$, $p < 0.0001$). Only SYFPEITHI at a saturated concentration was normal in ΔH2Mv mice (LSD: $p = 0.13$). Responses to ligands known to stimulate VSNs in the apical, *Vmn1r*-expressing layer (2-heptanone and isoamylamine) are not altered in ΔH2Mv mice (ns, nonsignificant; LSD: $p = 0.61$ and 0.78, respectively). Number of independent recordings is plotted in brackets above each bar. LSD: *$p < 0.05$; **$p < 0.01$; ***$p < 0.0001$. ***B***, Concentration dependency of EVG responses to rMUP25 in 129/Sv and ΔH2Mv mice. ***C–F***, Concentration-response curves constructed from EVG peak responses obtained in 129/Sv or ΔH2Mv mice ($n \geq 3$ each) to SEIDLILGY (***C***), f-MFFINTLTL (***D***), ESP1 (***E***), and rMUP25 (***F***). Responses induced by different concentrations of a ligand at a given recording position on the sensory surface of the VNE are normalized to the maximum response to this ligand measured at this position. Data are expressed as means ± SEM. The curves are fits of the Hill equation in combination with an iterative Levenberg–Marquardt nonlinear, least-squares fitting routine (χ^2 test: $p = 0.96 - 0.99$). The dashed and solid curves represent the mean concentration-response curve of 129/Sv and ΔH2Mv mice, respectively. EC_{50} values for 129/Sv and ΔH2Mv mice are, respectively: SEIDLILGY, $1.4 \pm 0.1 \cdot 10^{-13}$ M and $2.3 \pm 0.2 \cdot 10^{-12}$ M; f-MFFINTLTL, $3.1 \pm 0.3 \cdot 10^{-8}$ M and $4.4 \pm 0.3 \cdot 10^{-7}$ M; ESP1, $9.9 \pm 0.7 \cdot 10^{-10}$ M and $7.4 \pm 0.7 \cdot 10^{-9}$ M; rMUP25, $1.1 \pm 0.1 \cdot 10^{-9}$ M and $1.0 \pm 0.6 \cdot 10^{-8}$ M. Maximum responses to a given stimulus were not significantly different between 129/Sv and ΔH2Mv mice (LSD: $p = 0.07 - 0.64$), mean ± SEM μV (*n*): SEIDLILGY, 42.1 ± 5.0 (10) and 55.2 ± 7.9 (11); f-MFFINTLTL, 32.8 ± 6.4 (5) and 41.7 ± 7.2 (7); ESP1, 30.3 ± 3.2 (14) and 38.3 ± 2.8 (23); rMUP25, 40.1 ± 3.7 (12) and 36.7 ± 4.7 (13). Asterisks indicate significant differences between the genotypes at a specific concentration (LSD: *$p < 0.05$; **$p < 0.01$; ***$p < 0.0001$). ***G***, Histogram summarizing the magnitude of the shift in EC_{50} ratios of EVG concentration-response curves with different ligands in ΔH2Mv mice compared with WT mice.

percentage of responding cells over total cells imaged is plotted in Figure 7*E* as a function of decreasing dilution/increasing concentration of the HMW fraction. Significant differences are seen at $1/10^3$ and 1/300 dilutions: a much smaller percentage of VSNs is responsive in ΔH2Mv compared with WT (LSD: $p < 0.01$). Figure 7*F* shows the percentage of cells with a particular activation threshold as a function of decreasing dilution of the HMW fraction. In WT mice, among 106/2061 cells that responded to the HMW fraction, 1% (1 cell) responded already at $1/10^5$, 8% (9 cells) first at $1/10^4$, 32% (34 cells) at $1/10^3$, 36% (38 cells) at 1/300, and, finally, 23% (24 cells) only at $1/10^2$. The response map shows a pronounced rightward shift in ΔH2Mv mice: 0% (0 cells), 3% (2 cells), 6% (5 cells), 42% (36 cells), and 49% (42 cells) for a total of 85 responding cells, respectively. Within a certain concentration range ($1/10^5$ to $1/10^4$ dilution), there appear to be almost no responding VSNs in ΔH2Mv mice.

Thus, these experiments provide a third demonstration of the decreased sensitivity and higher activation thresholds of single VSNs in ΔH2Mvs mice using a mixture of natural ligands that are contained in the HMW fraction of urine.

AOB *in vivo* activation analyzed by c-Fos

We examined *in vivo* c-Fos activation in the AOB of WT and ΔH2Mv females after oronasal exposure to ESP1, a polypeptide that enhances female sexual receptivity upon male mounting: lordosis (Haga et al., 2010). WT females responded to 1 μM ESP1 with robust c-Fos immunoreactivity in some neurons of AOB mitral and granule cell layers, but this activity was virtually absent in ΔH2Mv mice (Fig. 7*G–I*). A concentration of 100 μM ESP1 produced much more activity in the AOB of ΔH2Mv mice. No activity was observed with the vehicle control. Thus, *in vivo* activation of the AOB is severely decreased in ΔH2Mv females when exposed to a low concentration of ESP1, but a higher ESP1 concentration can overcome this deficit, at least partially.

Behavioral phenotypes

Our physiological studies reveal a consistent phenotype: VSNs of ΔH2Mv mice display a decreased sensitivity, ranging from 8- to 34-fold, to individual chemoligands and natural urinary cues. We next investigated whether these cellular phenotypes are associated with alterations in VNO-dependent behaviors of ΔH2Mv mice that are exposed to WT mice or their chemosignals.

We measured male-male territorial aggression in a 10 min resident-intruder test (Fig. 8*A–C*). Urine samples, their low-molecular-weight or HMW fractions, or PBS as control were swabbed on the back of a castrated (nonaggressive) C57BL/6 male that was then introduced to a cage in which a single male, 129/Sv WT or ΔH2Mv, is housed. Aggression of the resident male toward the intruder male was measured by the parameters of attack duration (Fig. 8*A*), number of attacks during the 10 min period (Fig. 8*B*), and latency to first attack (Fig. 8*C*). We find that ΔH2Mv males show a pronounced decrease in aggression, with short and very few attacks, of which the first takes longer to occur.

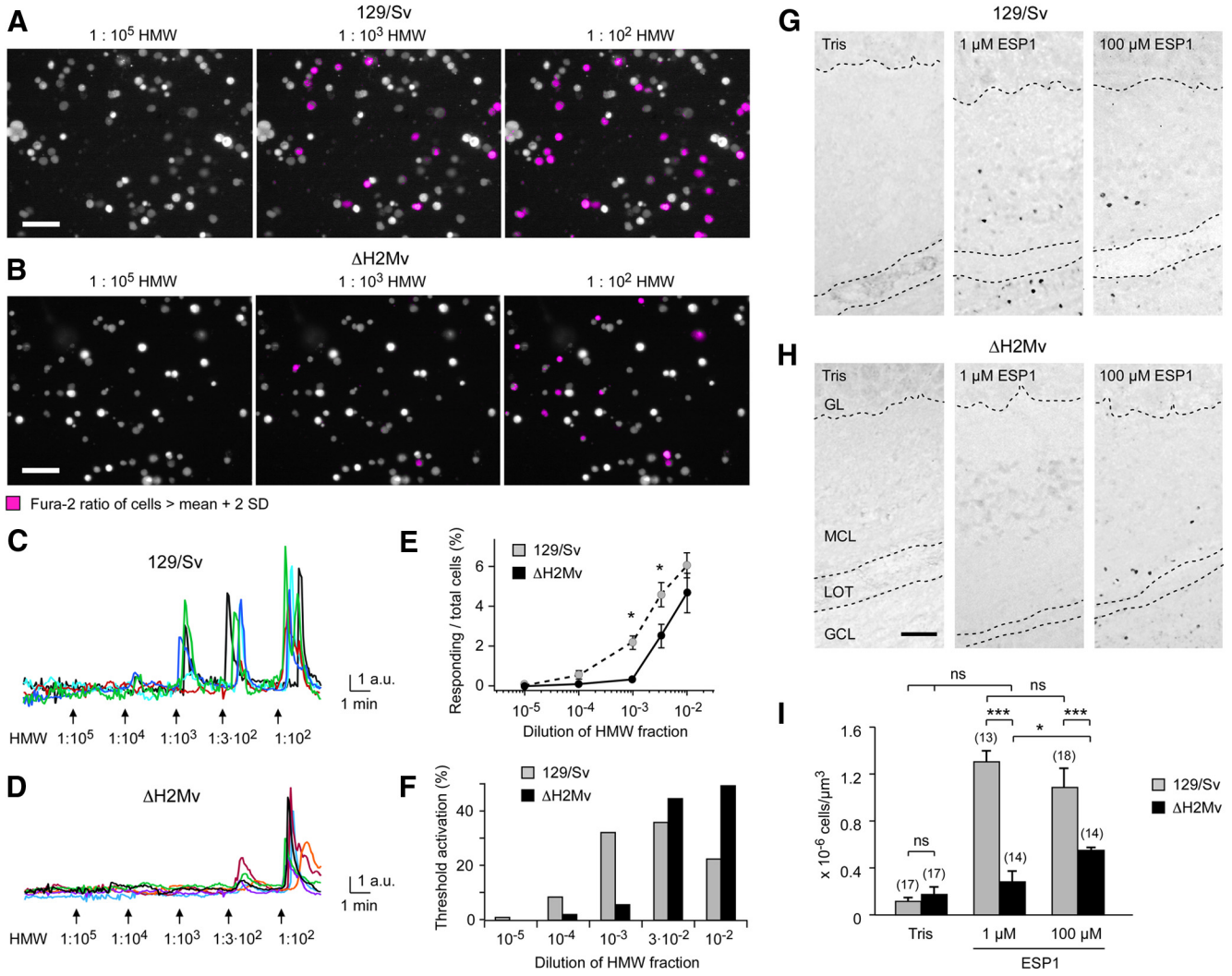

Figure 7. Calcium imaging in populations of dissociated VSNs and c-Fos analysis in AOB. ***A***, ***B***, Images of Fura-2 ratio responses (magenta) superimposed on gray scale Fura-2 images (taken at 380 nm before stimulation) in dissociated VSNs from 129/Sv (***A***) and ΔH2Mv mice (***B***). Cells were stimulated with various dilutions of HMW urine fractions. Scale bar, 50 μm. ***C***, ***D***, Concentration dependency of HMW-induced Ca^{2+} responses to decreasing dilutions of HMW fractions imaged in individual VSNs from 129/Sv (***C***) or ΔH2Mv (***D***). Examples from six VSNs per genotype are shown. Arrows indicate the time points at which the 30 s stimulus was turned on. ***E***, The percentage of responding cells over total cells increases with increasing concentrations of HMW fractions (ANOVA: $F_{(4,129)} = 43.03, p < 0.0001$). Significantly more 129/Sv cells responded at 10^{-3} and $3{\cdot}10^{-2}$ dilution of HMW urine fraction compared with ΔH2Mv cells (ANOVA: $F_{(1,129)} = 12.59, p < 0.01$; LSD: $^*p < 0.01$). Data are expressed as means ± SEM. At 10^{-2} dilution of HMW fraction, there is no significant difference between the two genotypes (LSD: $p = 0.16$). Criteria for Ca^{2+} responses in dissociated VSNs: a response is defined as an increase in fluorescence ratio to >1.5-fold of baseline; cells showing a response to control buffer were excluded from analysis, cells that responded to low but not to higher HMW concentrations were excluded and a response had to occur within 30 s after stimulus application. ***F***, Plot of threshold activation, defined as percentage of responsive cells beginning to respond at a given dilution of the HMW urine fraction, in 129/Sv vs ΔH2Mv mice. For each genotype, the percentages of the five bars add up to 100. ***G***, ***H***, Analysis of *in vivo* c-Fos activation in the AOB of WT or ΔH2Mv females following oronasal exposure to vehicle control (Tris) or 1 or 100 μM ESP1. Sagittal sections derive from the middle third of caudal AOB. GL, Glomerular layer; MCL, mitral cell layer; LOT, lateral olfactory tract; GCL, granule cell layer. Scale bar, 50 μm. ***I***, Quantification of c-Fos positive nuclei in the MCL ($n = 3$ females per condition and strain). The number of sections evaluated is indicated above each column. ANOVA: $F_{(5,92)} = 50.02, p < 0.0001$; LSD: $^{***}p < 0.0001$; $^*p < 0.05$; ns, not significant. Error bars represent means ± SEM.

Our cellular results in ΔH2Mv mice (sensitivity shift, but same maximum responses) predict that the level of male-male aggression in ΔH2Mv males should increase when higher stimulus concentrations are used. Indeed, a 4-fold higher concentration of HMW fraction (4× HMW) overcomes and rescues the aggression defect of ΔH2Mv males (Fig. 8*A–C*).

To examine maternal aggression, we used the same test against a castrated C57BL/6 intruder male with a lactating 129/Sv or ΔH2Mv female as resident. This test works best with total urine samples. We find that lactating ΔH2Mv females show a pronounced decrease in aggression toward the intruder male by the same three parameters (Fig. 8*D–F*). Pup retrieval, a maternal behavior that is not dependent on the VNO (Bean and Wysocki, 1989), is normal in ΔH2Mv females (Fig. 8*G*).

We also measured lordosis behavior by females. A single-housed 129/Sv, WT, or ΔH2Mv female is exposed for 30 min to a sexually experienced C57BL/6 male, which will try to mount her. The female often displays dorsiflexion of her vertebral column to facilitate copulation. We find that ΔH2Mv females show a pronounced decrease in lordosis, as measured by the occurrence of lordosis in response to mounting (the lordosis quotient; Fig. 8*H*), the percentage of females that display a lordotic response (Fig. 8*I*), and the duration of lordosis (Fig. 8*J*). Males show no difference in the latency to first mount of 129/Sv or ΔH2Mv females (Fig. 8*K*) and 129/Sv or ΔH2Mv females exhibit equal durations of investigation of the male anogenital region (Fig. 8*L*).

Thus, VNO-dependent behaviors are severely impaired in ΔH2Mv mice; in both males and females, there is a pronounced

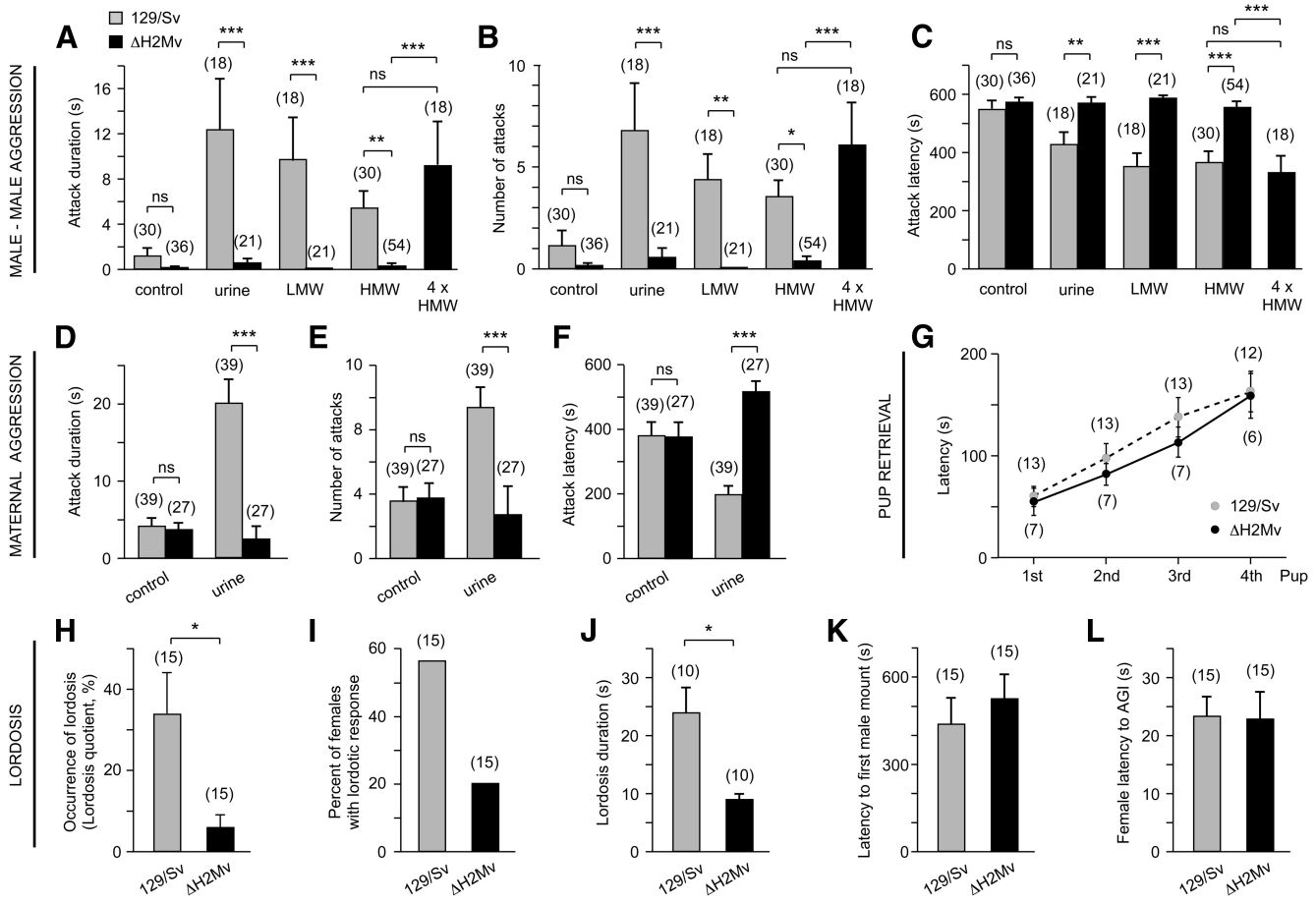

Figure 8. Behavioral deficits in male and female ΔH2Mv mice. ***A–C***, Impaired male-male aggression in ΔH2Mv mice. Attack duration (***A***; ANOVA: $F_{(8,245)} = 7.635$, $p < 0.0001$), number of attacks (***B***; ANOVA: $F_{(8,245)} = 7.903$, $p < 0.0001$), and latency to first attack (***C***; ANOVA: $F_{(8,245)} = 12.894$, $p < 0.0001$) in 129/Sv males ($n = 10$) compared with ΔH2Mv males ($n = 18$). A 4-fold increase in the concentration of HMW fraction (4× HMW) rescued the aggression defect in ΔH2Mv males. LSD: ***$p < 0.0001$; **$p < 0.01$; *$p < 0.05$; ns, not significant. ***D–F***, Impaired maternal aggression in lactating ΔH2Mv females. Attack duration (***D***; ANOVA: $F_{(3,131)} = 15.79$, $p < 0.0001$), number of attacks (***E***; ANOVA: $F_{(3,131)} = 6.887$, $p < 0.0001$), and latency to first attack (***F***; ANOVA: $F_{(3,131)} = 12.688$, $p < 0.0001$) in 129/Sv females ($n = 13$) compared with ΔH2Mv females ($n = 9$). Castrated intruder males were swabbed with 40 μl of saline solution (control), urine, low molecular weight urine, or HMW urine fractions. Number of individual measurements is indicated in brackets above each bar. Each value consists of three repeated measurements, performed on different days, per mouse. LSD: ***$p < 0.0001$; ns, not significant. ***G***, Pup retrieval abilities do not differ significantly between lactating 129/Sv ($n = 13$) and ΔH2Mv ($n = 7$) females (ANOVA: $F_{(1,77)} = 0.92$, $p = 0.34$). Error bars represent mean ± SEM. ***H–L***, Impaired lordosis behavior of ΔH2Mv females. The lordosis quotient (LQ) is the ratio of the number of lordosis postures shown by a female in response to a fixed number of mounts multiplied with 100. The LQ is significantly decreased in ΔH2Mv females (*t* test: *$p < 0.05$; ***H***). This decrease is most likely due to the low percentage of ΔH2Mv females showing lordosis behavior compared with the 129/Sv females (***I***). The duration of lordosis behavior in ΔH2Mv females is also decreased (***J***; *t* test: **$p < 0.01$). In contrast, there is no difference in latency to first male mounting (***K***; *t* test: $p = 0.58$) and female investigation of the anogenital region of males (ANI; ***L***; *t* test: $p = 0.97$).

decrease in quantitative measures of aggressive and sexual behaviors. A higher HMW concentration can overcome the deficit in male-male aggression.

Discussion

More than a decade since the initial reports about the *H2-Mv* genes and their VSN-specific, combinatorial expression patterns (Ishii et al., 2003; Loconto et al., 2003), there was still no information about the *in vivo*, physiological roles of H2-Mvs. The obvious knock-out experiment was long overdue but complicated due to the need to inactivate nine genes at once; it is unlikely that a single *H2-Mv* gene knock-out would be informative, because multiple *H2-Mv* genes are coexpressed in combinations within individual VSNs. We have previously applied the chromosome engineering technique to delete a 600 kb cluster of 16 *Vmn1r* genes (Del Punta et al., 2002a) to provide the first genetic evidence for a physiological role of Vmn1rs in pheromone responses. The ΔH2Mv mice lack a genomic region of 530 kb that encompasses the nine *H2-Mv* genes but no other genes. Their vomeronasal system does not show overt anatomical defects; if it were grossly malformed, such as if VSN axons did not form glomeruli in the AOB, then the results of the physiological and behavioral experiments would have been much less interpretable. Our anatomical analyses rule out a major role for H2-Mvs in VSN axonal wiring and coalescence into glomeruli. Subtle defects in VSN survival and in synapse function and stability in the AOB remain to be explored.

Half of basal, *Vmn2r*-expressing VSNs do not coexpress *H2-Mv* Genes

It is frequently overlooked that only half of the basal, *Vmn2r*-expressing VSNs coexpress *H2-Mv* genes. A generalized and absolute dependence of Vmn2rs or Vmn2r-expressing VSNs on H2-Mvs can therefore be excluded from first principles. The VNE displays a tripartite layered organization (Ishii and Mombaerts, 2008), with VSNs in the basal part of the basal, *Vmn2r*-expressing VNE layer coexpressing the nine *H2-Mv* genes, but not VSNs in the apical part of the basal, *Vmn2r*-expressing VNE layer. A given

family-ABD *Vmn2r* gene (115 in total) is expressed in either the basal or apical part of the basal layer, but not in both parts. Because these two parts are approximately equal in size, it follows that approximately half of basal VSNs, possibly expressing half of family-ABD *Vmn2r* genes, do not coexpress *H2-Mv* genes. VSNs in both parts of the basal layer coexpress one to six members of the seven family-C *Vmn2r* genes, in nonrandom combinations (Silvotti et al., 2007, 2011; Ishii and Mombaerts, 2011). RNA expression of the three family-C *Vmn2r* genes for which we could design NanoString probes (*Vmn2r1*, *Vmn2r3*, and *Vmn2r4*) is normal at 3 and 8 weeks. We have characterized in depth one family-ABD *Vmn2r* gene for each part of the basal layer: we have generated gene-targeted strains and identified MHC peptide ligands for *Vmn2r26* (=*V2r1b*), which is expressed in the apical part without *H2-Mv* genes and without another family-ABD *Vmn2r* gene, and for *Vmn2r81* (*V2rf2*), which is expressed in the basal part together with *H2-Mv* genes and without another family-ABD *Vmn2r* gene. *Vmn2r116* (*V2Rp5*) is expressed in basal VSNs that respond to ESP1 (Kimoto et al., 2005), is required for physiological ESP1 responses (Haga et al., 2010), and is coexpressed with *M10.1* through *M10.6* (Haga et al., 2007). The subcellular localization of V2Rp5 immunoreactivity and the numbers of V2Rp5-immunoreactive cells are comparable between ΔH2Mv and WT mice.

Molecular Vmn2r/H2-Mv interactions

Our data provide genetic evidence that H2-Mvs are not absolutely essential for VSNs to generate physiological responses to chemostimuli, but are required for their ultrasensitivity. In sharp contrast, the responses of V2r1b- or V2rf2-expressing VSNs to MHC peptides depend absolutely on an intact *Vmn2r* locus (Leinders-Zufall et al., 2009; present results). Thus, cells that transcribe a disrupted *Vmn2r* locus that no longer encodes the protein do not respond to these peptides, whereas in the absence of H2-Mvs, these responses still do occur. Unfortunately, sensitivity or affinity of Vmn2r receptors cannot be determined directly, certainly not in native VSNs. It is therefore not possible to infer specific models for conceivable molecular Vmn2r-H2-Mv interactions (Olson et al., 2006) from our physiological data. What can be studied with the available methods and reagents is the physiological sensitivity of the VSNs that express these Vmn2rs by measuring parameters that are downstream from receptor binding, such as increases in intracellular Ca^{2+} and local field potentials. A conservative conclusion is that the decreased sensitivity of VSNs from ΔH2Mv mice to chemoligands and the comparable maximum responses exclude an absolute requirement for H2-Mv molecules as chaperones or escort molecules for Vmn2rs that are normally coexpressed with them. Our data also rule out that the actual and exclusive receptors for chemoligands are the H2-Mvs themselves.

Cell-autonomous action of H2-Mvs

The single-cell results from V2rf2-GFP and V2r1b-GFP mice indicate that the decrease in physiological sensitivity is a cell-autonomous phenotype: the ΔH2Mv mutation affects only cells that express these genes normally in WT mice. The phenotypes are thus not due to systemic or nonspecific effects of the ΔH2Mv mutation. *V2rf2*, a family-ABD *Vmn2r* gene, is not coexpressed with another family-ABD gene and is coexpressed with Vmn2r1 (family C) in most cells at 10 weeks; NanoString counts for *Vmn2r1* are normal both at 3 and 8 weeks. Therefore, the decreased sensitivity of single V2rf2-GFP cells to peptide ligands is not the result of decreased expression in other *Vmn2r* genes of either family ABD or family C. The decrease in V2rf2-GFP cell counts in a mixed genetic background does not affect the interpretation of the single-cell results. Because there is no significant difference in the NanoString counts for *Vmn2r* genes at 3 weeks and a small fraction of *Vmn2r* genes shows a decrease at 8 weeks, we speculate that the decreased physiological sensitivity can result, over time, in a net cell loss of certain VSN subsets, perhaps due to decreased cell survival.

Behavioral deficits

Our tests of aggressive and sexual behaviors reveal profound impairments in ΔH2Mv males and females. The male–male aggression deficit can be overcome by increasing the concentration of the urinary HMW fraction from the standard 1× to 4×, suggesting that VSN sensitivity is finely calibrated to a biologically relevant window of concentrations of urinary chemostimuli. These results highlight the importance of stimulus intensity in instructing VSN-dependent behavioral responses (He et al., 2010; Arnson and Holy, 2013). They also indicate the need to maintain ultrahigh sensitivity of stimulus recognition for proper behavioral responses, which is consistent with the extremely low concentrations of some natural stimuli in urine (Sturm et al., 2013). These behavioral tests imply that only few components of the urinary HMW fraction, which may be detected at similar thresholds, could be sufficient to elicit male–male aggression.

Although the behavioral deficits are consistent with the strong decrease in physiological sensitivity of VSNs, they are perhaps not caused solely by this decreased sensitivity. We cannot rule out a contribution by a decrease in the numbers of certain VSN subsets and/or the *Vmn2r* RNA/Vmn2r protein level per cell. In any case, these decreases in an inbred background are relatively minor: there is a 25% decrease in the number of cells that react with the *V2rf1-3* ISH probe (labeling *Vmn2r80*, *Vmn2r81*, and *Vmnr82*) and only 3/36 (8%) of assayable *Vmn2r* genes show a substantial decrease in NanoString analysis at 8 weeks. There is no significant difference in the number of activated cells and the size of EOG population responses when saturating stimulus intensities are used, suggesting that the impact of cell loss in ΔH2Mv mice is relatively minor in our functional experiments. Regardless of the mechanisms underlying the behavioral deficits, we have here provided evidence that H2-Mv genes are required for normal patterns of VNO-related behaviors.

Conclusion and a look ahead

H2-Mvs have been proposed to be involved in Vmn2r receptor localization and trafficking or, more directly, in the process of pheromone detection in VSNs expressing these molecules (Dulac and Torello, 2003; Loconto et al., 2003). However, because only half of Vmn2r-expressing VSNs coexpress *H2-Mvs* normally, a priori, there cannot be a general dependence of Vmn2rs on H2-Mvs. Based on the proposal of Loconto et al. (2003), physiological responses of VSNs to chemostimuli (MHC peptides, ESP1, MUPs) would have been expected to be absent in ΔH2Mv mice, but that is not the case: H2-Mvs are not absolutely essential for physiological responses to chemostimuli to be generated in VSNs. Instead, we observe a decreased sensitivity, with comparable maximum responses. We have thus provided genetic evidence that H2-Mvs contribute to ultrasensitive chemodetection of these VSNs.

There is no knowledge regarding the densities of Vmn2r receptors, G-proteins, and other signaling elements in the membrane of VSN microvilli, in contrast to the detailed quantitative information for photoreceptor cells (Yau and Hardie, 2009). Un-

til such information becomes available, our results can be interpreted in terms of multiple functional models at the cellular and biochemical level. It remains to be determined whether the sensitivity shift that we observe in single cells reflects a direct interaction of H2-Mv proteins with Vmn2r proteins, a decrease in Vmn2r protein expression on the surface of VSN microvilli, or both. Several mechanistic hypotheses remain to be explored.

References

Adams EJ, Luoma AM (2013) The adaptable major histocompatibility complex (MHC) fold: structure and function of nonclassical and MHC class I-like molecules. Annu Rev Immunol 31:529–561. CrossRef Medline

Arnson HA, Holy TE (2013) Robust encoding of stimulus identity and concentration in the accessory olfactory system. J Neurosci 33:13388–13397. CrossRef Medline

Bean NJ, Wysocki CJ (1989) Vomeronasal organ removal and female mouse aggression: the role of experience. Physiol Behav 45:875–882. CrossRef Medline

Bufe B, Schumann T, Zufall F (2012) Formyl peptide receptors from immune and vomeronasal system exhibit distinct agonist properties. J Biol Chem 287:33644–33655. CrossRef Medline

Chamero P, Marton TF, Logan DW, Flanagan K, Cruz JR, Saghatelian A, Cravatt BF, Stowers L (2007) Identification of protein pheromones that promote aggressive behaviour. Nature 450:899–902. CrossRef Medline

Chamero P, Katsoulidou V, Hendrix P, Bufe B, Roberts R, Matsunami H, Abramowitz J, Birnbaumer L, Zufall F, Leinders-Zufall T (2011) G protein Gαo is essential for vomeronasal function and aggressive behavior in mice. Proc Natl Acad Sci U S A 108:12898–12903. CrossRef Medline

Chamero P, Leinders-Zufall T, Zufall F (2012) From genes to social communication: molecular sensing by the vomeronasal organ. Trends Neurosci 35:597–606. CrossRef Medline

Del Punta K, Leinders-Zufall T, Rodriguez I, Jukam D, Wysocki CJ, Ogawa S, Zufall F, Mombaerts P (2002a) Deficient pheromone responses in mice lacking a cluster of vomeronasal receptor genes. Nature 419:70–74. CrossRef Medline

Del Punta K, Puche A, Adams NC, Rodriguez I, Mombaerts P (2002b) A divergent pattern of sensory axonal projections is rendered convergent by second-order neurons in the accessory olfactory bulb. Neuron 35:1057–1066. CrossRef Medline

Dey S, Matsunami H (2011) Calreticulin chaperones regulate functional expression of vomeronasal type 2 pheromone receptors. Proc Natl Acad Sci U S A 108:16651–16656. CrossRef Medline

Dulac C, Torello AT (2003) Molecular detection of pheromone signals in mammals: from genes to behaviour. Nat Rev Neurosci 4:551–562. CrossRef Medline

Edgar R, Domrachev M, Lash AE (2002) Gene Expression Omnibus: NCBI gene expression and hybridization array data repository. Nucleic Acids Res 30:207–210. CrossRef Medline

Haga S, Kimoto H, Touhara K (2007) Molecular characterization of vomeronasal sensory neurons responding to a male-specific peptide in tear fluid: sexual communication in mice. Pure Applied Chemistry 79:775–783. CrossRef

Haga S, Hattori T, Sato T, Sato K, Matsuda S, Kobayakawa R, Sakano H, Yoshihara Y, Kikusui T, Touhara K (2010) The male mouse pheromone ESP1 enhances female sexual receptive behavior through a specific vomeronasal receptor. Nature 466:118–122. CrossRef Medline

He J, Ma L, Kim S, Schwartz J, Santilli M, Wood C, Durnin MH, Yu CR (2010) Distinct signals conveyed by pheromone concentrations to the mouse vomeronasal organ. J Neurosci 30:7473–7483. CrossRef Medline

Ishii T, Mombaerts P (2008) Expression of nonclassical class I major histocompatibility genes defines a tripartite organization of the mouse vomeronasal system. J Neurosci 28:2332–2341. CrossRef Medline

Ishii T, Mombaerts P (2011) Coordinated coexpression of two vomeronasal receptor V2R genes per neuron in the mouse. Mol Cell Neurosci 46:397–408. CrossRef Medline

Ishii T, Hirota J, Mombaerts P (2003) Combinatorial coexpression of neural and immune multigene families in mouse vomeronasal sensory neurons. Curr Biol 13:394–400. CrossRef Medline

Ishii T, Omura M, Mombaerts P (2004) Protocols for two- and three-color fluorescent RNA in situ hybridization of the main and accessory olfactory epithelia in mouse. J Neurocytol 33:657–669. CrossRef Medline

Khan M, Vaes E, Mombaerts P (2011) Regulation of the probability of mouse odorant receptor gene choice. Cell 147:907–921. CrossRef Medline

Khan M, Vaes E, Mombaerts P (2013) Temporal patterns of odorant receptor gene expression in adult and aged mice. Mol Cell Neurosci 57:120–129. CrossRef Medline

Kimoto H, Haga S, Sato K, Touhara K (2005) Sex-specific peptides from exocrine glands stimulate mouse vomeronasal sensory neurons. Nature 437:898–901. CrossRef Medline

Leinders-Zufall T, Zufall F (2013) The electrovomeronasogram: field potential recordings in the mouse vomeronasal organ. Methods Mol Biol 1068:221–236. CrossRef Medline

Leinders-Zufall T, Lane AP, Puche AC, Ma W, Novotny MV, Shipley MT, Zufall F (2000) Ultrasensitive pheromone detection by mammalian vomeronasal neurons. Nature 405:792–796. CrossRef Medline

Leinders-Zufall T, Brennan P, Widmayer P, S PC, Chandramani PS, Maul-Pavicic A, Jäger M, Li XH, Breer H, Zufall F, Boehm T (2004) MHC class I peptides as chemosensory signals in the vomeronasal organ. Science 306:1033–1037. CrossRef Medline

Leinders-Zufall T, Cockerham RE, Michalakis S, Biel M, Garbers DL, Reed RR, Zufall F, Munger SD (2007) Contribution of the receptor guanylyl cyclase GC-D to chemosensory function in the olfactory epithelium. Proc Natl Acad Sci U S A 104:14507–14512. CrossRef Medline

Leinders-Zufall T, Ishii T, Mombaerts P, Zufall F, Boehm T (2009) Structural requirements for the activation of vomeronasal sensory neurons by MHC peptides. Nat Neurosci 12:1551–1558. CrossRef Medline

Loconto J, Papes F, Chang E, Stowers L, Jones EP, Takada T, Kumánovics A, Fischer Lindahl K, Dulac C (2003) Functional expression of murine V2R pheromone receptors involves selective association with the M10 and M1 families of MHC class Ib molecules. Cell 112:607–618. CrossRef Medline

Logan DW, Marton TF, Stowers L (2008) Species specificity in major urinary proteins by parallel evolution. PLoS ONE 3:e3280. CrossRef Medline

Martini S, Silvotti L, Shirazi A, Ryba NJ, Tirindelli R (2001) Co-expression of putative pheromone receptors in the sensory neurons of the vomeronasal organ. J Neurosci 21:843–848. Medline

Mombaerts P, Wang F, Dulac C, Chao SK, Nemes A, Mendelsohn M, Edmondson J, Axel R (1996) Visualizing an olfactory sensory map. Cell 87:675–686. CrossRef Medline

Mudge JM, Armstrong SD, McLaren K, Beynon RJ, Hurst JL, Nicholson C, Robertson DH, Wilming LG, Harrow JL (2008) Dynamic instability of the major urinary protein gene family revealed by genomic and phenotypic comparisons between C57 and 129 strain mice. Genome Biol 9:R91. CrossRef Medline

Olson R, Dulac C, Bjorkman PJ (2006) MHC homologs in the nervous system – they haven't lost their groove. Curr Opin Neurobiol 16:351–357. CrossRef Medline

Ramírez-Solis R, Liu P, Bradley A (1995) Chromosome engineering in mice. Nature 378:720–724. CrossRef Medline

Rivière S, Challet L, Fluegge D, Spehr M, Rodriguez I (2009) Formyl peptide receptor-like proteins are a novel family of vomeronasal chemosensors. Nature 459:574–577. CrossRef Medline

Silvotti L, Moiani A, Gatti R, Tirindelli R (2007) Combinatorial coexpression of pheromone receptors, V2Rs. J Neurochem 103:1753–1763. CrossRef Medline

Silvotti L, Cavalca E, Gatti R, Percudani R, Tirindelli R (2011) A recent class of chemosensory neurons developed in mouse and rat. PLoS ONE 6:e24462. CrossRef Medline

Sturm T, Leinders-Zufall T, Maček B, Walzer M, Jung S, Pömmerl B, Stevanović S, Zufall F, Overath P, Rammensee HG (2013) Mouse urinary peptides provide a molecular basis for genotype discrimination by nasal sensory neurons. Nat Commun 4:1616. CrossRef Medline

Vaes E, Khan M, Mombaerts P (2014) Statistical analysis of differential gene expression relative to a fold change threshold on NanoString data of mouse odorant receptor genes. BMC Bioinformatics 15:39. CrossRef Medline

Walz A, Rodriguez I, Mombaerts P (2002) Aberrant sensory innervation of the olfactory bulb in neuropilin-2 mutant mice. J Neurosci 22:4025–4035. Medline

Yau KW, Hardie RC (2009) Phototransduction motifs and variations. Cell 139:246–264. CrossRef Medline

Zufall F, Kelliher KR, Leinders-Zufall T (2002) Pheromone detection by mammalian vomeronasal neurons. Microsc Res Tech 58:251–260. CrossRef Medline